Funded by
the European Union

Horizon Europe

EUROPEAN COMMISSION

European Climate, Infrastructure and Environment Executive Agency (CINEA)

Grant agreement no. 101056765

Electric Vehicles Management for carbon neutrality in Europe

Deliverable D2.3
Optimal management of V2X in parking lots

Document Details

Due date	29-02-2024
Actual delivery date	30-04-2024
Lead Contractor	Technical University of Denmark (DTU)
Version	1.0
Prepared by	Jan Engelhardt (DTU), Anna Malkova (DTU), Xihai Cao (DTU), Pietro Zunino (DTU), Jan Martin Zepter (DTU), Charalampos Ziras (DTU), Mattia Marinelli (DTU), Benedikt Baldursson (CC), Maria Hach (BEOF), Herbert Amezquita (INESC), Cindy P. Guzman (INESC), Hugo Morais (INESC)
Reviewed by	Igor Mendek (UL), George Papadakis (PPC)
Dissemination Level	Public

Project Contractual Details

Project Title	Electric Vehicles Management for carbon neutrality in Europe
Project Acronym	EV4EU
Grant Agreement No.	101056765
Project Start Date	01-06-2022
Project End Date	30-11-2025
Duration	42 months

Document History

Version	Date	Contributor(s)	Description
0.1	6th Nov 2023	DTU	Table of contents
0.2	14th Dec 2023	DTU	Draft File
0.3	17th Apr 2024	DTU, CC, BEOF, INESC ID	Version for internal review
1.0	30th Apr 2024	DTU, CC, BEOF, INESC ID	Version after internal review

Disclaimer

Acknowledgment

This document is a deliverable of EV4EU project. EV4EU has received funding from the European Union´s Horizon Europe programme under grant agreement no. 101056765.

Funded by
the European Union

[1] https://ev4eu.eu/

Executive Summary

The present deliverable D2.3 presents the modelling framework and research backbone to the development of Vehicle-to-Everything (V2X) strategies for the demonstration activities in Denmark as part of the EV4EU project. The charging infrastructure at both locations of the Danish demo (Risø and Campus Bornholm) is identical and comprises six Alternating Current (AC) chargers with two connectors (dual outlet) providing 11 kW charging power each. The twelve charge points are connected to the grid with a maximum cluster power limit of 43 kW. The developed V2X strategies aim to provide a seamless integration of the charging infrastructure in the electricity system and serve two main purposes. Firstly, they ensure the compliance with the grid connection limit, as the cluster limit of 43 kW is lower than the sum of the rated power of all charge points. Secondly, they utilize the flexibility of charging processes to provide services both behind and in front of the meter.

The modelling framework comprised forecast models to predict the Electric Vehicle (EV) charging demand, as well as the expected generation from local Renewable Energy Sources (RES). The forecast models were integrated in the control models developed within the scope of this work. Moreover, users of the charging infrastructure at the Danish demo sites can provide their estimated departure time and energy needs via an app, which is taken into account in the decision-making process.

The control models facilitate the coordination of EV charging, which offers the possibility to provide services to local and external grids. This is tested through a set of different scenarios and control objectives. The conducted simulations utilize actual Photovoltaic (PV) production and EV charging data from winter and summer weeks in Denmark. It is shown that the proposed control methods achieve the compliance with local grid connection limits and are further able to provide demand response to Distribution System Operators (DSOs) by reducing the cluster power limit temporarily and on request. The tested reduction of the cluster power limit by half from 43 kW to 21.5 kW on weekdays between 7 a.m. and 12 p.m. leads to a decrease of the fulfilled energy requested by the EVs by 5% in the summer scenario and 6% in the winter scenario. Yet, this decrease is small considering that the power reduction is requested for 5 consecutive hours with frequent EV arrivals. The consideration of local PV generation, as present at the demo site Campus Bornholm, allows to cover parts of the EV charging demand through local generation from RES. In the summer scenario, an overall proportion of 77% of the energy delivered to EVs is provided by the local PV system, defining the system's self-sufficiency. Conversely, 27% of the total energy provided by the local PV system is utilized for EV charging, defining the system's self-consumption. In the winter scenario, the values for self-sufficiency and self-consumption are 13% and 84%, respectively.

In case single-phase EVs are present in charging clusters, the charging processes can lead to phase unbalances. To counteract this effect, the present work proposes an approach for including phase unbalance constraints in the optimization problem formulation and demonstrates its functionality through simulations. Moreover, the technical capability of EV charging infrastructure to provide frequency control was assessed. The work investigated a distributed control method utilizing the autonomous controllability of the chargers deployed in the Danish demonstration. The model parameters, such as delays from hardware and software, were characterized through the installation at Risø Campus. The simulation results showed that the distributed control architecture enables on average a 9% faster response compared to the centralized method and followed the reference value more closely.

The developed control methods serve as a basis for the upcoming demonstrations in Work Package 9 (WP9). In this regard, the experimental testing is expected to provide important insights on how the proposed methods perform within real operational settings.

Table of Contents

List of Figures

List of Tables

List of Acronyms

AC	Alternating Current
AWS	Amazon Web Services
CA	Cloud Aggregator
CC	Circle Consult
DK2	Danish Bidding Zone 2
DSO	Distribution System Operator
DTU	Technical University of Denmark
EV	Electric Vehicle
EV4EU	Electric Vehicles Management for carbon neutrality in Europe
LightGBM	Light Gradient Boosting Machine
LP	Linear Problem
NRMSE	Normalized Root Mean Square Error
PCC	Point of Common Coupling
PV	Photovoltaic
PWM	Pulse-Width Modulation
RES	Renewable Energy Source
SOC	State of Charge
TS	Time Stamp
TSO	Transmission System Operator
UR	Update Rate
V2X	Vehicle to Everything
VA	Virtual Aggregator
WB	Whiteboard

1 Introduction

The availability of Electric Vehicles (EV) charging infrastructure at parking lots is an integral part in the transition to electric transportation. Management systems employing Vehicle-to-Everything (V2X) strategies offer a seamless integration of charging infrastructure in the electricity system, utilizing the fact that charging processes are commonly flexible in time. The present deliverable D2.3 presents the modelling framework and research backbone to the development of V2X strategies for the demonstration activities in Denmark described in Work Package 9 (WP9).

1.1 Scope and objectives

The management system used for the charging infrastructure in the Danish demonstration serves two main purposes. Firstly, it ensures the compliance with grid connection limits, as the power rating at the Point of Common Coupling (PCC) is lower than the sum of the rated power of all chargers. Secondly, it utilizes the flexibility of charging processes to provide services both behind and in front of the meter.

In particular, the presented control models facilitate cost-optimized charging, the utilization of local renewables, and phase balancing. Furthermore, service provision is investigated in the form of demand response programs for Distribution System Operators (DSOs), and frequency control for Transmission System Operators (TSOs). Additionally, the unique technical capabilities of the chargers deployed in the Danish demonstration are captured. The chargers are equipped with local controllers that can make autonomous decisions, which enables both centralized and distributed control architectures for the charging cluster.

The modelling framework further employs forecast models to predict the EV charging demand (consumption side), and the expected generation from a local Photovoltaic (PV) system (production side). These forecast models are integrated in the control models developed within the scope of this task.

1.2 Relationship with other deliverables

The work of this task is linked to D9.1 *Use case specification, development, installation, commissioning, demonstration, and evaluation planning for the Danish demo* [1], as this previous deliverable specified the properties of the parking lot cluster investigated in D2.3. Similarly, the experimental demonstration conducted in WP9 and reported in its respective deliverables D9.2 – D9.5 will utilize the control models explored in D2.3.

The present task builds up on the previous deliverables of WP2. The Danish cluster setup was also considered in a building context as part of D2.2 *Control strategies for V2X integration in buildings* [2]. Moreover, the EV forecast model employed in D2.3 is based on D2.1 *Control Strategies for V2X Integration in Houses* [3] and D2.2 *Control Strategies for V2X Integration in Buildings* [2]. Subsequent deliverables in WP2 are D2.4, D2.5, and D2.6.

1.3 Structure

The present document is divided into four sections. After this introduction, Section 2 provides an overview of the EV cluster setup at the locations of the Danish demonstration.
Section 3 forms the main body of the deliverable and presents the developed forecast and control models, as well as the investigated scenarios. Firstly, Section 3.1 introduces a forecast model to predict EV charging demand at specific locations, based on historical data. Section 3.2 is dedicated to a control model optimizing the charging processes within EV clusters to comply with grid connection limits, provide demand response, or utilize local RES. In Section 3.3, the focus is moved to how to incorporate phase unbalance constraints in EV load management systems to mitigate the impact of single-phase EV charging. Section 3.4 explores the technical feasibility of providing frequency control with a distributed control architecture and compares the performance to a centralized management system. Finally, Section 4 concludes the deliverable summarizing its key findings.

2 Setup description

The EV charging cluster setup deployed as part of the Danish demonstration comprises six Alternated Current (AC) chargers, each of which provides a maximum current of 32 A per phase, corresponding to a power of 22 kW. The chargers have two outlets, providing the opportunity for twelve EVs to be connected at the same time. The charging infrastructure is integrated via a 63 A grid connection (43 kW). Figure 1 provides an overview of the setup.

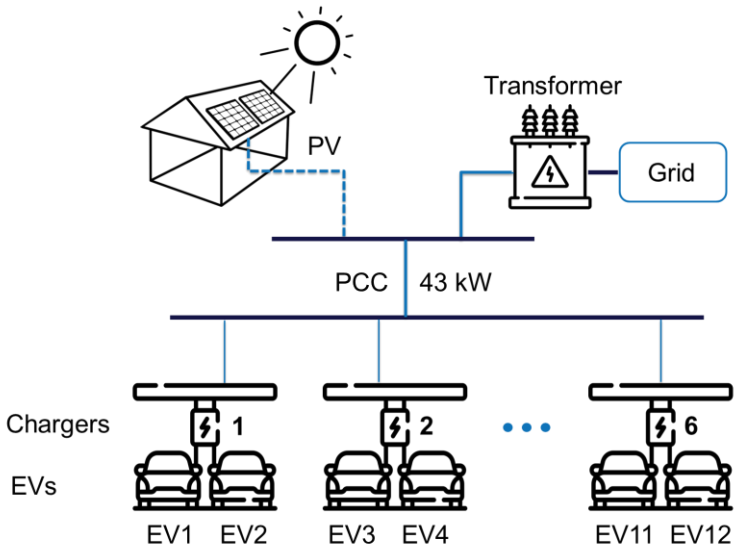

Figure 1: Charging cluster setup at the Danish demo locations Risø and Campus Bornholm. The setup is identical at both locations, except for a PV system, which is only present at Campus Bornholm.

The Danish demonstration takes place at two different locations – Risø and Campus Bornholm. Risø is a research campus of Technical University of Denmark (DTU) and located in Roskilde, while Campus Bornholm is an educational institute in the main town Rønne on the island of Bornholm. The charging infrastructure deployed at both locations is identical and shown in Figure 1. Each of the twelve charge points (six chargers with two outlets each) will provide charge power up to 11 kW. At a later stage of the demonstration, the operation of each charger aims at offering a flexible allocation of the 22 kW to its two outlets. This might make it possible to charge at 22 kW in case only one of the two outlets is occupied. However, since this operation of the chargers has not been tested yet, the studies conducted as part of the present deliverable assume a maximum charging power of 11 kW per charge point. The charger design and the installation at Risø Campus is shown in Figure 2. For more details on the infrastructure deployed as part of the Danish demonstration the interested reader is referred to deliverable D9.1 [1].

The parking lot at Risø is used by employees of DTU and not publicly accessible. The location is used for testing the chargers and control methods in an enclosed environment and allows for preliminary quantification of control parameters, as further described in Section 3.4. The location Campus Bornholm is publicly accessible and will be used by residents of the island, tourists, as well as students and employees of the educational institute. The location further offers the possibility to utilize a local PV plant to partially, or at times fully, cover the consumption from EVs. This will be further assessed in Section 3.2.

Users of the charging infrastructure will start their charging sessions through an app, which is developed by Circle Consult (CC) as part of the Electric Vehicles Management for carbon neutrality in Europe (EV4EU) project. The app allows the user to provide key inputs, such as the anticipated parking time and the required energy, which enable the load management system to consider user preferences while controlling the overall cluster consumption. The app is also used for the payment system. The data acquisition and logging further include high-resolution power measurements at each charger, and of the overall cluster consumption through a dedicated meter at the PCC

Each charger deployed in this project is equipped with a controller that enables the charger to make autonomous control decisions. This facilitates distributed control schemes where all chargers are provided with global quantities, such as the cluster reference power and the actual cluster consumption, based on which all chargers individually control their respective charging session to collectively meet the cluster requirements.

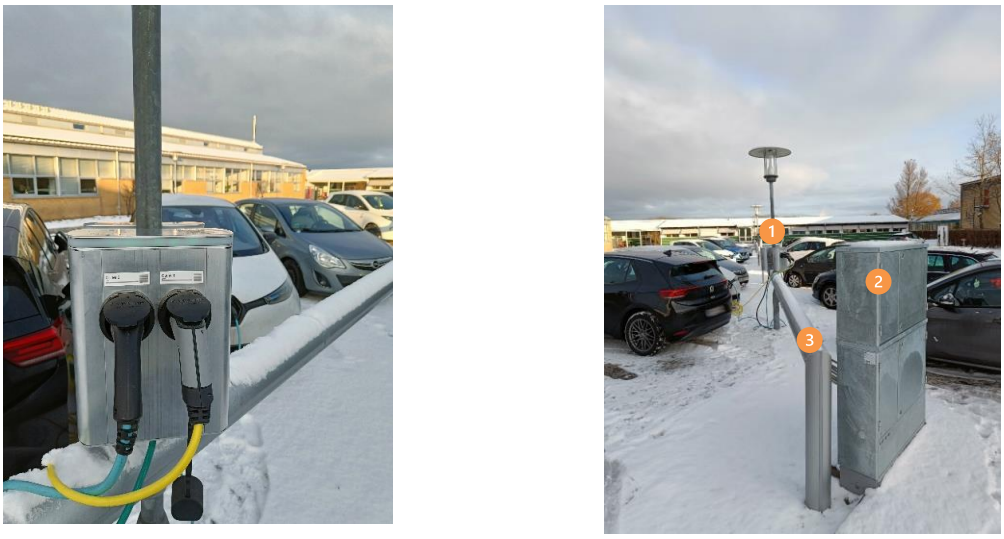

a) b)

Figure 2: Charging cluster setup. a) Charger design with two outlets per charger; b) Installation at Risø Campus (1: Chargers; 2: PCC cabinet; 3: Cable tube for connecting chargers to PCC cabinet).

3 Control model and simulation results

This section presents the forecast and control models developed as part of T2.3. Firstly, Section 3.1 introduces a forecast model to predict EV charging demand at specific locations. Section 3.2 is dedicated to a control model optimizing the charging processes within EV clusters. This control model is tested for three different scenarios: complying with grid connection limits, demand response initiated by the DSO, and utilization of local Renewable Energy Sources (RES). Section 3.3 presents a method for incorporating phase unbalance constraints in EV load management systems. Finally, Section 3.4 explores the technical feasibility of providing frequency control with a distributed control architecture.

3.1 EV forecast model

Two different datasets (DTU and Public Power Corporation (PPC)) are used to perform cluster power forecasting. In both cases, the defined cluster corresponds to the aggregated power for a specific number of chargers. The DTU dataset is from a public research and educational campus in Lyngby, Denmark. The PPC dataset is from a charging cluster in Athens, Greece. The forecasting is calculated for the entire cluster power, rather than the individual chargers. Two scenarios are simulated for both datasets, forecasting one week in summer (August) and one week in winter (January). The forecast model used corresponds to Light Gradient Boosting Machine (LightGBM) [4], an open-source gradient boosting framework developed by Microsoft that is designed for efficiency, high performance, and scalability [5]. LightGBM was selected, since it was used in the previous deliverables D2.1 [2] and D2.2 [3]. The features used in the model are the lags (target values from previous periods) for 1, 5 and 7 days, the hour and the day of the year. These features were chosen after a feature selection approach based on the correlation matrix. The metric used to evaluate forecast performance is the Normalized Root Mean Square Error (NRMSE)[6], formulated as follows:

$$NRMSE = \frac{\sqrt{\sum_{i=1}^{N} \frac{(y\,predicted_i - y\,actual_i)^2}{N}}}{y_{max} - y_{min}}$$

Where N is the total number of values in the test set, $y\,predicted$ is the forecasted value, $y\,actual$ is the true value, y_{max} is the maximum true value and y_{min} is the minimum true value.

The forecasting model was developed in Python and the results obtained for each dataset are presented as follows.

3.1.1 DTU dataset

The DTU cluster consists of 12 chargers: 6499-1, 6499-2, 6500-1, 6500-2, 6501-1, 6502-1, 6502-2, 6503-1, 6503-2, 7584-1, and 7584-2. The available data spans almost one year, from 2022-09-05 to 2023-08-20. Figure 3 presents the power timeseries for the DTU cluster.

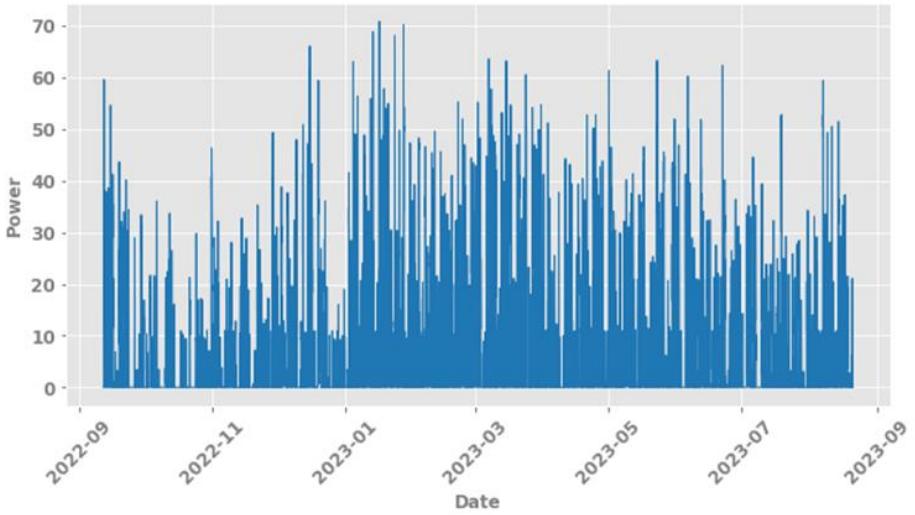

Figure 3: Power timeseries DTU cluster.

Figure 4 presents the forecast results obtained for the summer scenario. In this case, the data from 2022-09-12 to 2023-07-31 was used for training and the first week of August 2023 was forecasted. The NRMSE achieved by the LightGBM model was 11.6%, which represents a 35% improvement compared to the NRMSE obtained by the Persistence (Naive) model, which was 18%.

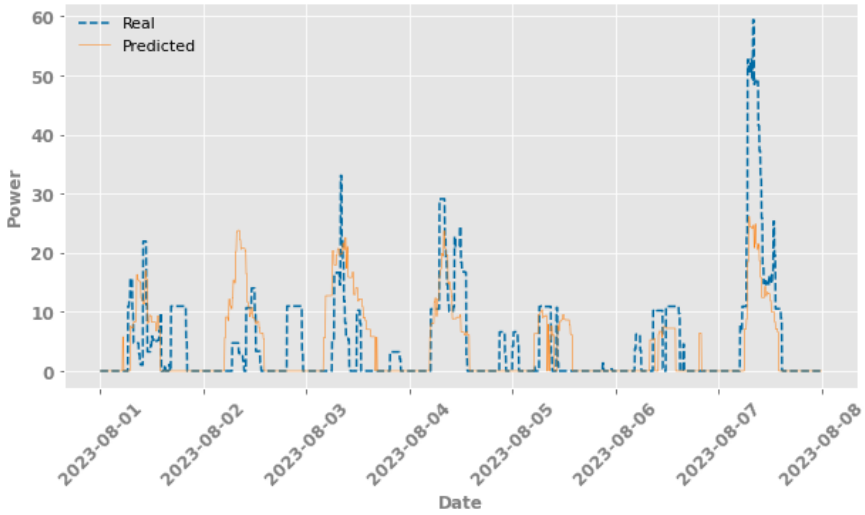

Figure 4: Forecast results for summer scenario DTU cluster.

Figure 5 presents the forecast results obtained for the winter scenario. In this case, the data from 2022-09-12 to 2023-01-01 was used for training and the first week of January 2023 was forecasted. The NRMSE achieved by the LightGBM model was 18%, which represents a 10% improvement compared to the NRMSE obtained by the Persistence (Naive) model, which was 20%.

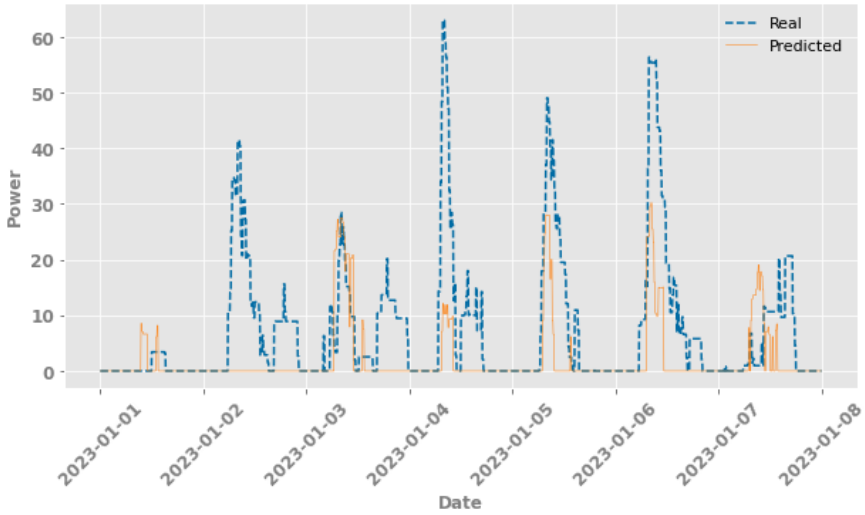

Figure 5: Forecast results for winter scenario DTU cluster.

The difference in the forecast accuracy between the summer and winter scenarios for the DTU dataset can be attributed to the quantity of data available for training. In the summer scenario, the model was trained with almost one year of data capturing a wide range of seasonal patterns and fluctuations in EV power consumption. Conversely, in the winter scenario, the training data covered a comparatively shorter period, just 4 months, limiting the model's exposure to winter-specific consumption patterns and therefore obtaining a higher error. This discrepancy underscores the importance of data quantity in forecasting accuracy, as a greater volume of training data enables models to capture more nuanced trends and seasonal variations, ultimately enhancing predictive performance.

3.1.2 PPC Dataset

The PPC cluster consists of twelve chargers: KOMERAX1, KOMERAX3, KOMERAX5, KOMERAX6, KOMERAX7, KOMERAX8, KOMERAX9, KOMERAX10, KOMERAX11, KOMERAX14, KOMERAX17 and KOMERAX18. The available data spans almost one year and a half, from 2022-07-18 to 2024-01-31. Figure 6 presents the power tim

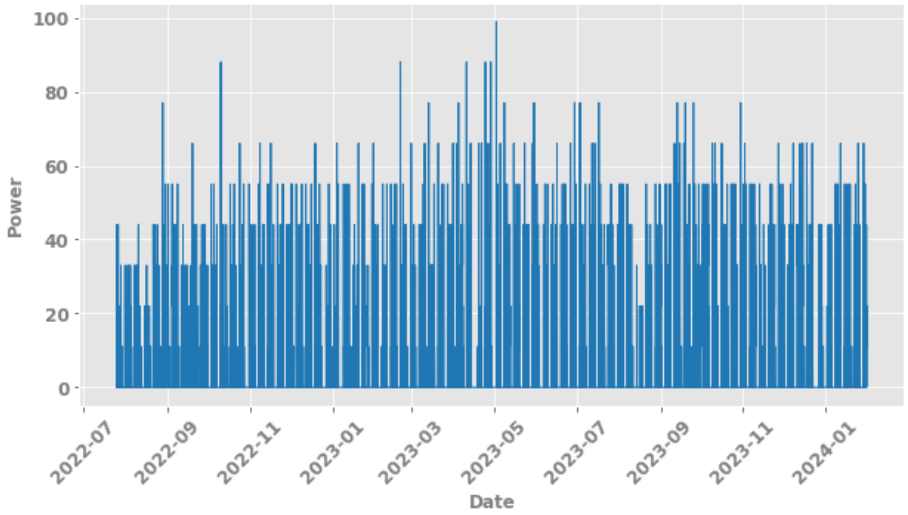

Figure 6: Power timeseries PPC cluster.

Figure 7 presents the forecast results obtained for the summer scenario. In this case, the data from 2022-07-25 to 2023-07-31 was used for training and the first week of August 2023 was forecasted. The NRMSE achieved by the LightGBM model was 10.5%, which represents a 34% improvement compared to the NRMSE obtained by the Persistence (Naive) model, which was 16%.

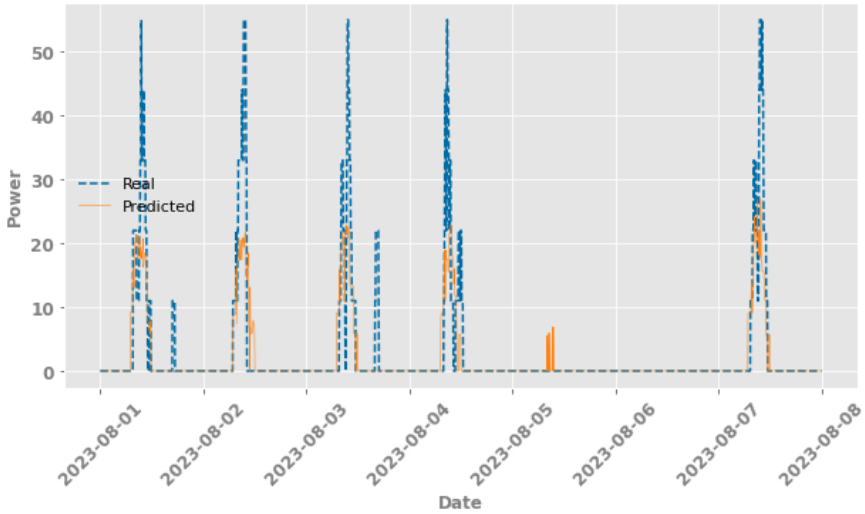

Figure 7: Forecast results for summer scenario PPC cluster.

Figure 8 presents the forecast results obtained for the winter scenario. In this case, the data from 2022-07-25 to 2023-12-31 was used for training and the first week of January 2024 was forecasted. The NRMSE achieved by the LightGBM model was 9.5%, which represents a 37% improvement compared to the NRMSE obtained by the Persistence (Naive) model, which was 15%.

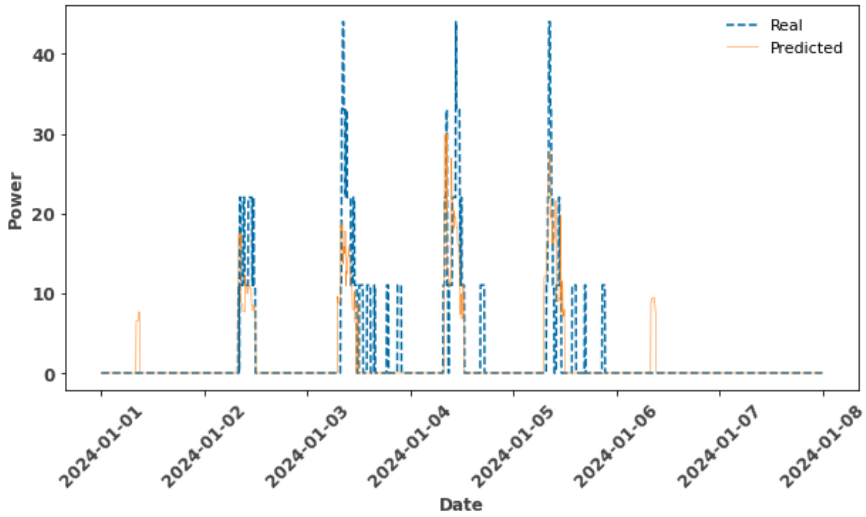

Figure 8: Forecast results for winter scenario PPC cluster.

The results of the EV charging behaviour forecast model are used as an input for the control model presented in the following section.

3.2 Control model for EV load management

The present section presents the control model developed for providing load management of the charging cluster. Firstly, the methodology is described, detailing the mathematical formulation. Secondly, the simulation scenarios are introduced along with the metrics for quantifying the performance of the model. Finally, the simulation results for the different scenarios are presented and discussed.

3.2.1 Methodology

In this section, the methodology of the model is introduced in two subsections. Firstly, the general structure of the model is described as well as the rolling horizon algorithm applied to the model. Secondly, the mathematical formulation of an optimization problem used in a model core is shown and explained.

3.2.1.1 General model structure

The structure of the model is shown in Figure 9. The model consists of two core sub-models: the upper-level model and the lower-level model. The upper-level model is a main component of charging station operation, while the lower-level is mainly used for validation of upper-level model decisions. The initial parameters, case settings, simulation time horizon (considered time of model run) and other auxiliary variables are set before the model run and thus lay outside of the rolling horizon block seen in Figure 9. Then, inside the rolling horizon loop the prices, PV data, EV cluster considered data and EV database are continuously updated at every model run. The model is structured to be able for continuous run adaptation for further test validations. The first three inputs are then going to the upper-level model, so it can base decisions on them. The upper-level model is a Linear Problem (LP) optimization model

with a cost minimization objective. It produces the P_{ref} for the whole charging station treating the chargers as one cluster of loads.

The power reference is then used as a maximum allowed power input to the lower-level model. The lower-level model is a power-sharing model, which dispatches allowed P_{ref} equally among the connected EVs. It receives the information about EV from the EV database which is updated on an event basis (EV is connected, disconnected). An EV will always comply with its maximum power limitations, and therefore if dispatched power to this EV is higher than its capability it will stick to its power limits. As described in Section 2, each charge point has a power rating of 11 kW.

To facilitate the EV energy request compliance the anonymous feedback loop is introduced. At every model run the lower model calculates the minimum necessary power for each EV needed for the next steps to deliver 100% of the energy request for the EV. Then the sum of these power minimums is sent to the upper-level model as a minimum limit for P_{ref} allocation. This is the only information which goes from the lower-level model (and thus EVs) to the upper-level model. The upper level has no access to any inputs from EVs. This is done to comply with the anonymous approach of data security and further investigations on a lower level are done with distributed control, thus it will not store information at one node of computation. This helps to ensure information security and single-point failure.

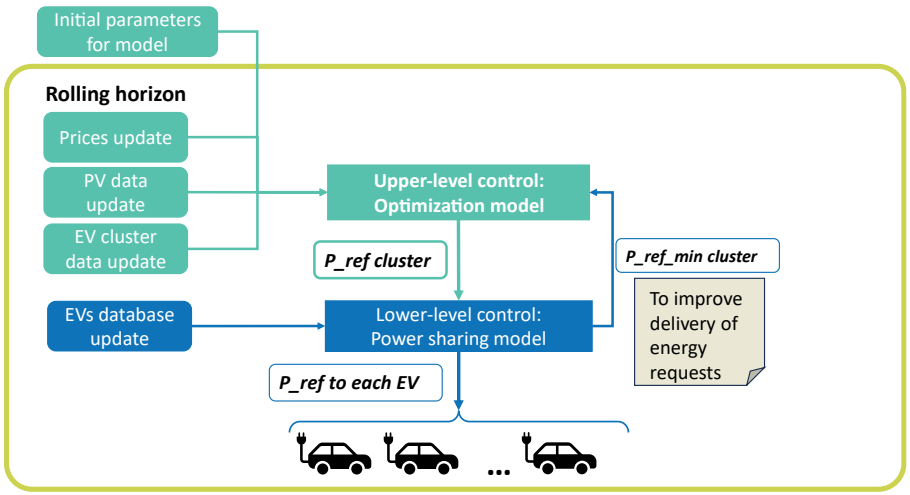

Figure 9: General model structure scheme.

The rolling horizon algorithm is shown in Figure 10. First, the simulation time horizon is set. From the specified dates for which the model should run the simulation and the periodicity of runs (Δt) the number of model run steps τ is calculated. The future goal is to put the model in online mode, so everything will be happening in real time. The optimization horizon is the horizon of the model foreseen to the future and the decisions it takes at each run. Only the prices are 100% certain for the model's observation of the horizon as they were published on the previous day. The model is tuned to run for a week of the simulation horizon (overall run timeframe), and six hours for the optimization horizon (model observations, forecasts and decisions) with a periodicity of runs equal to five minutes. Every five minutes in simulation time the model runs and produces the $P_{ref\ t,h}$ for the cluster for the next 73 steps (current step plus next six hours making it 1 plus 72 steps). However, the model implements only the $P_{ref\ t,1}$, which is the decision for the current step. Then, the horizon moves

further. The rest of $P_{ref\ t,h}$ is not needed while the model runs without any issues. However, for future considerations of the field model implementation if the error occurs the power reference will take the last allocated $P_{ref\ t,h}$ decision for the next six hours.

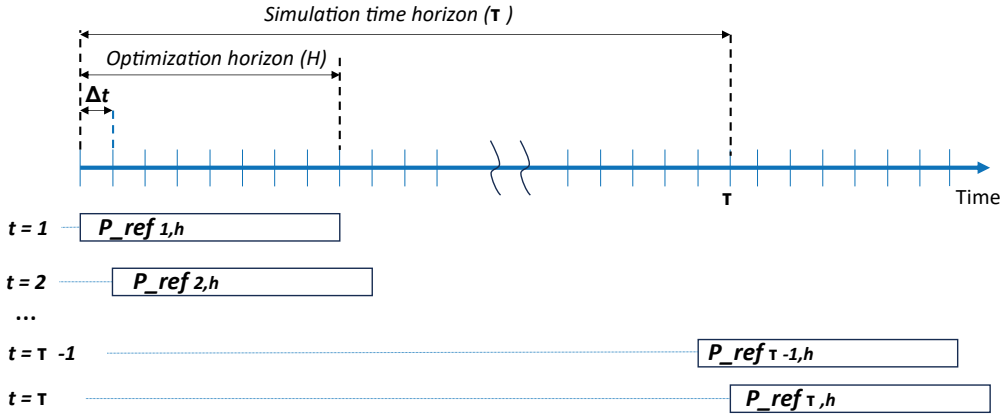

Figure 10: Rolling horizon algorithm scheme.

3.2.1.2 Mathematical formulation of optimization problem

The simulation time horizon and optimization horizon are set to a week and six hours correspondingly with a five-minute resolution. Thus, the simulation steps are $t = 1,2 \dots \tau = 1,2 \dots 2016$; and optimization horizon steps are $h = 1,2 \dots H = 1,2 \dots 73$. Below variables and parameters for the optimization model are introduced in Table 1.

Table 1: List of variables and parameters of the optimization model.

Variables		Parameters and Scalars	
$P_{t,h}^{\text{cluster}}$	decision variable, the power reference for the whole cluster. The output of the upper-level model is a maximum limit for the lower level.	$C_{t,h}^{\text{import}}, C_{t,h}^{\text{export}}$	vectors of import and export prices
E_t^{cluster}	variable of charging energy with decided power references for the cluster within the horizon time. It is necessary to ensure energy compliance with the required energy preserved for the cluster within the horizon.	$P_{t,h}^{\text{PV}}$	vector of PV data input to the model
$P_{t,h}^{\text{grid}}$	variable of throughput at the transformer.	$P_t^{\min}, P_t^{\max}$	minimum and maximum cluster power values. The minimum is set by the lower-level model as feedback from EV charging needs.
		P_{trafo}^{max}	Maximum is set to the transformer's maximum power of $P_{trafo}^{max} = 43\ kW$ or less if DSO gives the command.

$\boldsymbol{P}_{t,h}^{\mathbf{import}}, \boldsymbol{P}_{t,h}^{\mathbf{export}}$	variables of $P_{t,h}^{grid}$ decomposition depending on whether the power throughput is positive (importing) or negative (exporting).	$P_{t,h}^{forecast}$	vector of forecasted power consumption by EVs
$\boldsymbol{f}_{t,h}^{\mathbf{import}}, \boldsymbol{f}_{t,h}^{\mathbf{export}}$	binary variables preventing the model from simultaneously importing and exporting power through the transformer.	$E_t^{required}$	minimum amount of energy to deliver with power reference decision. Based on forecasted power consumption by EVs

Objective function

The objective function aims to minimize costs (maximize own benefit):

$$\min \sum_{H} \left(C_{t,h}^{\text{import}} \cdot \boldsymbol{P}_{t,h}^{\mathbf{import}} + C_{t,h}^{\text{export}} \cdot \boldsymbol{P}_{t,h}^{\mathbf{export}} \right)$$

Where, $C_{t,h}^{import}$ is a total import price including spot price, grid tariffs, and taxes, while $C_{t,h}^{export}$ is only the spot price. Thus, local renewable excess production is sold at a lower price than drawing energy from the grid.

Constraints:

- Transformer throughput decomposition constraints:

$$\begin{aligned} \boldsymbol{P}_{t,h}^{\mathbf{grid}} &= \boldsymbol{P}_{t,h}^{\mathbf{import}} + \boldsymbol{P}_{t,h}^{\mathbf{export}}, && \forall t \in T, h \in H \\ 0 \leq \boldsymbol{P}_{t,h}^{\mathbf{import}} &\leq \boldsymbol{f}_{t,h}^{\mathbf{import}} \cdot P_{trafo}^{max}, && \forall t \in T, h \in H \\ -\boldsymbol{f}_{t,h}^{\mathbf{export}} \cdot P_{trafo}^{max} &\leq \boldsymbol{P}_{t,h}^{\mathbf{export}}, && \forall t \in T, h \in H \\ \boldsymbol{f}_{t,h}^{\mathbf{import}} + \boldsymbol{f}_{t,h}^{\mathbf{export}} &\leq 1, && \forall t \in T, h \in H \end{aligned}$$

  These constraints ensure the power limitations of the transformer for import and export and prevent the model from simultaneous import and export.

- Power balance constraint:

$$\boldsymbol{P}_{t,h}^{\mathbf{cluster}} = P_{t,h}^{\text{PV}} + \boldsymbol{P}_{t,h}^{\mathbf{grid}}, \qquad \forall t \in T, h \in H$$

- Cluster power consumption limitations constraint:

$$P_{t,h}^{\min} \leq \boldsymbol{P}_{t,h}^{\mathbf{cluster}} \leq P_t^{\max}, \qquad \forall t \in T, h \in H$$

- Energy delivery constraints:

$$\begin{aligned} \boldsymbol{E}_t^{\mathbf{cluster}} &= \sum_{H} \boldsymbol{P}_{t,h}^{\mathbf{cluster}} \cdot \Delta t, && \forall t \in T \\ E_t^{\text{required}} &\leq \boldsymbol{E}_t^{\mathbf{cluster}}, && \forall t \in T \end{aligned}$$

These constraints force the model to deliver the required amount of energy for the charging station. The required energy is calculated as follows:

$$E_t^{\text{required}} = \sum_H P_{t,h}^{\text{forecast}} \cdot \Delta t, \qquad \forall t \in T$$

A more thorough explanation of the model methodology will be published in paper [7].

3.2.1.3 Model inputs

Every run mode updates necessary inputs.

- Prices are decomposed into import and export prices. The import prices include spot prices from the Danish bidding zone 2 (DK2) and Danish dynamic grid tariffs. The export price however includes only spot prices. Elafgift (electricity tax) and value-added tax are excluded in the considerations.

- EV power consumption forecast is done using machine learning algorithms, as described in Section 3.1. The initial historical data are from DTU charging station recordings at Lyngby Campus.

- The EV database is a summary of recorded charging sessions at the DTU charging station. The database is updating on an event basis, meaning EV inputs are occurring there only when EVs are connected and deleted from the database when they are disconnected. The EV input data includes arriving time, leaving time, maximum power consumption capability of EV, and energy request.

- PV data consists of a PV forecast and PV measurement. For the PV forecast the persistence forecast is used meaning that the PV measurements from the previous day are taken for the PV forecast of the current day. PV data is then obtained in the following way: PV power is measured at the time of the model run and this value is then fixed for half an hour in model consideration as the most probable value for PV output. However, the rest time of the optimization horizon is still the PV persistence forecast. A deeper explanation of PV data can be found in [8], which describes the previous version of the model with shrinking horizon optimization. Figure 11 shows PV data logic production.

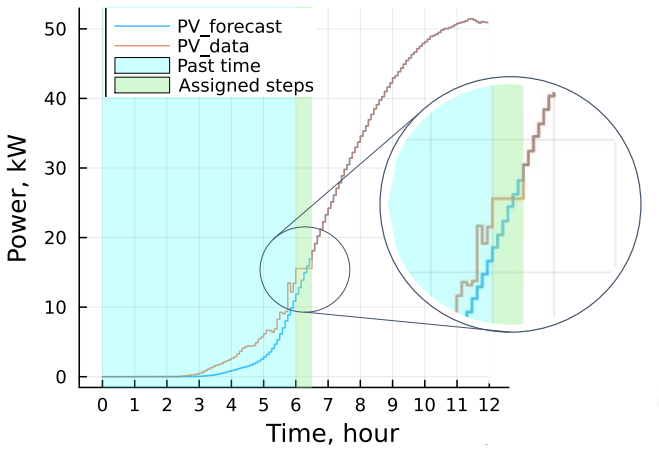

Figure 11: PV data formulation at 6:00 AM.

3.2.2 Scenarios and metrics

The objective of the modelling activities in the scope of this deliverable is to test control methods that allow for using the flexibility from EV charging. To test the control model for EV load management, described in Section 3.3.1, the optimisation model is run for three scenarios that ensure thorough coverage of potential conditions and variables and showcase the functioning of the model. This section describes these scenarios and the specific input data needed. Specifically, the three scenarios comprise:

1. The compliance with a specific grid connection limit.
2. The facilitation of dynamic demand response for the DSO.
3. The integration of both dynamic electricity prices and local renewable energy sources.

The first scenario is related to the case where an EV charging cluster that is composed of, in this case, twelve charging outlets of which each can provide a charging power of up to 11 kW is connected to a physical grid connection limit (e.g., due to a fuse rating) of 43 kW. This grid connection limit is well below the cumulative charging power that the aggregate of all chargers could provide to the EVs. Hence, the model needs to facilitate an intelligent coordination of the charging processes of the EVs while respecting grid connection limits and the energy requests of the EV users.

The second scenario is connected to demand response provided for the DSO. Specifically, this scenario considers a temporary reduction of the maximum cluster power. Due to local network conditions, a DSO may require the EV cluster to reduce their charging power during specific times of the day. This could e.g. be the case in an industrial area where energy-intensive industrial processes are run during specific times of the day such that less capacity is available for the EV cluster in order not to overload the local distribution grid. As EV charging imposes a new electric load, the local distribution grid might not be sized accordingly to facilitate both. In the scope of this deliverable, it is exemplarily considered that the grid connection limit is reduced from 7 a.m. to 12 p.m. from 43 kW to 21.5 kW (50%). The control model hence needs to facilitate the fact that for a certain time window a lower charging power is available.

The third scenario is directed at the optimal operation of the EV cluster when considering both dynamic electricity prices and local renewable energy sources behind-the-meter. In this case, the model needs to decide what power reference to set throughout the day considering the forecasted production of photovoltaic and EV load. The scenario demonstrates the price-optimised EV load management for the charging cluster.

All scenarios have been run for a simulation horizon of one week in both summer and winter and hence allow for a performance evaluation with different levels of PV production. The metrics along which the model performance is assessed are:

- Energy delivery fulfilment to the EVs (in %)
- Cost of cluster operation (including revenues from selling to the grid, in €)
- Self-sufficiency and self-consumption of the EV cluster (in %)

3.2.3 Results and discussion

In this section, the simulation results are presented. The simulations are conducted both for the summer and winter weeks, however, graphically Scenarios 2 and 3 are presented only with the

summer case. For better observability only two days of the week are shown on plots: 2nd and 3rd of August 2023 and 2nd and 3rd of January 2023. Nevertheless, the final metric comparison at the end of the subsection is done for all three scenarios and for whole weeks in summer and winter, respectively.

3.2.3.1 Scenario 1: Compliance with grid connection limit

Figure 12 shows the power reference allocation decided for summer week 2023 for the first scenario. In this case, the PV panel is not considered in the model and the power reference fully follows the price signals and minimum power request from the EVs as well as the power consumption forecast. Thus, the model allocates the power reference at its biggest during the cheapest hours as it sees the prices for only the next six hours. The upper-level reference does not have any information about the actual cluster consumption but only the forecasted power consumption. Also, when EVs are present the upper-level receives the $P_{t,h}^{\min}$ signals that force it to allocate more power for EVs, therefore the power reference is at least $P_{t,h}^{\min}$, despite the prices being higher. The spikes the $P_{t,h}^{\min}$ are due to the approaching departure time of the individual EVs and their respective charging needs with shrinking time. The increasing urgency of charging lets $P_{t,h}^{\min}$ communicate to the upper control level increase. As apparent from the third subplot, the model considers individual charging sessions with different energy needs, arrival and departure times and maximum charging power. As seen from the Figure 12, the power reference is never set above the default cluster limit of 43 kW. Therefore, it can be concluded that the control model successfully complies with the set grid connection limit.

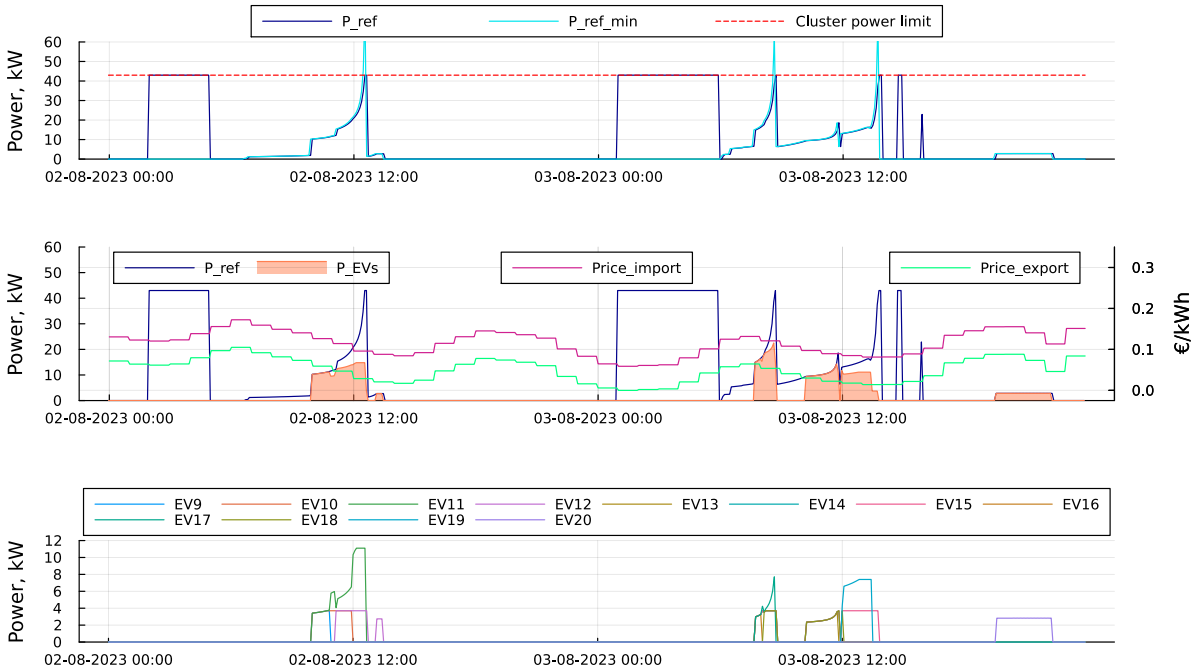

Figure 12: Upper: Power reference allocated with P_ref_min and cluster limit; middle: power reference with electricity prices and aggregated power consumption of EVs; down: power consumption of each EV.

3.2.3.2 Scenario 2: Dynamic demand response for the DSO

In this scenario, the cluster power limit is decreased by DSO command in particular time periods. It is considered that DSO commands the charging station to reduce their consumption two times from 43 kW to 21.5 kW in hours of expected high loading of the power grid on weekdays between 7:00 and 12:00 when the industrial processes experience peak loads. The results of the simulations are shown in Figure 13. The DSO command does not have any influence during the first observed day, as the power reference is below this limit during the power limitation command. However, on the second day plotted, the power reference is limited by the DSO command and despite the increasing power request $P_{t,h}^{\min}$ from the lower-level model, it does not go above specified DSO limits. The overall assessment of the charging fulfilment under limited cluster power is provided in the comparison of all scenarios at the end of this subsection.

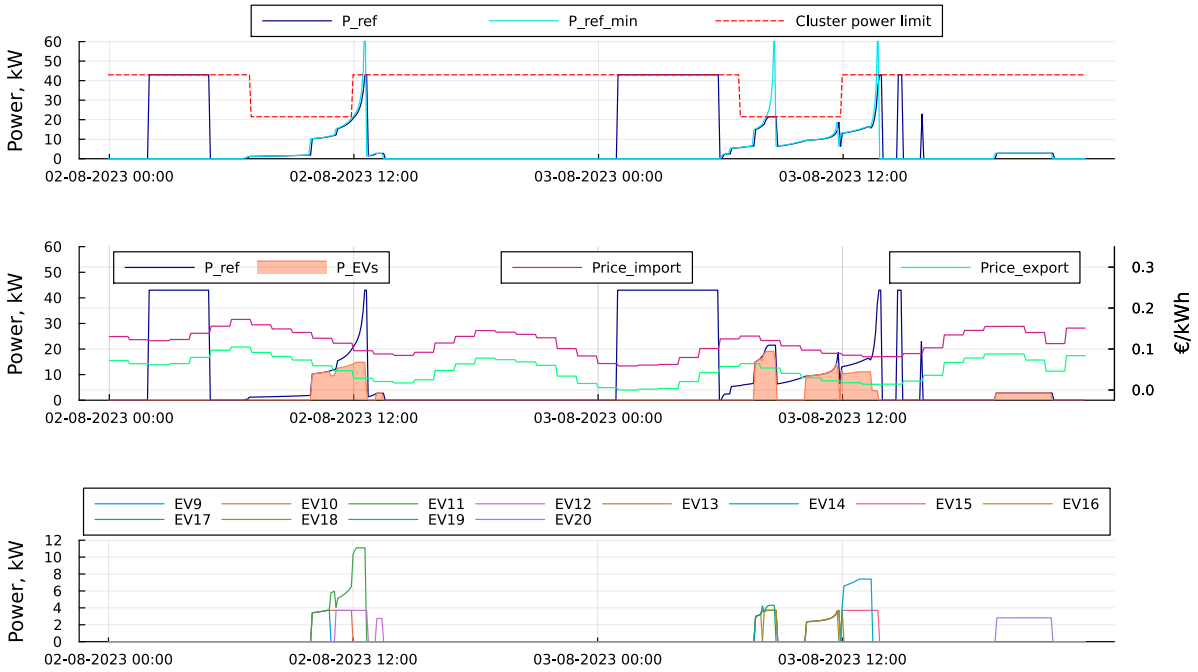

Figure 13: Upper: Power reference allocated with P_ref_min and cluster limit; middle: power reference with electricity prices and aggregated power consumption of EVs; down: power consumption of each EV.

3.2.3.3 Scenario 3: Integration of local RES

In this scenario, a PV system of 61 kWp is added to the charging station. To see the impact of photovoltaic generation, we will show the results for both summer and winter weeks. The PV production is considered without cost for local consumption. The PV production hence contributed to the local EV charging consumption at no cost, while import is priced at end-user consumption prices.

The summer week results for the 2nd and 3rd of August are introduced in Figure 14. The PV production measurements can be seen in the top plot of Figure 14 in orange. The power reference follows the measured PV production where economically reasonable. During the day, a large part of the PV

production is exported to the grid whenever it exceeds the consumption of the EV cluster to generate revenue for the charging cluster operator. As the charging processes coincide with the bell curve of PV production, most of the charging is covered by local generation.

To further explain the rationale behind the model decisions, Figure 15 presents the model output based on a forecasting optimization horizon of six hours at 06:00 and 12:00 for the 2nd of August 2023. In the upper plot for the 06:00 decision time (left figure), it is shown how the PV forecasts are integrated into the decision-making process. It can be appreciated how the reference power follows the predicted PV power for the complete horizon. As explained in Section 3.2.1, the actual PV measurements are overwriting the forecasts for the next half an hour (as can be seen by the first six time steps). The quantity E_required is based on the forecast model described in Section 3.1, and varies depending on the predicted load. From the plot at 12:00, it can be seen that the reference power follows P_ref_min. This is due to the communication of minimum charging power requirements from the lower-level model to the upper-level model.

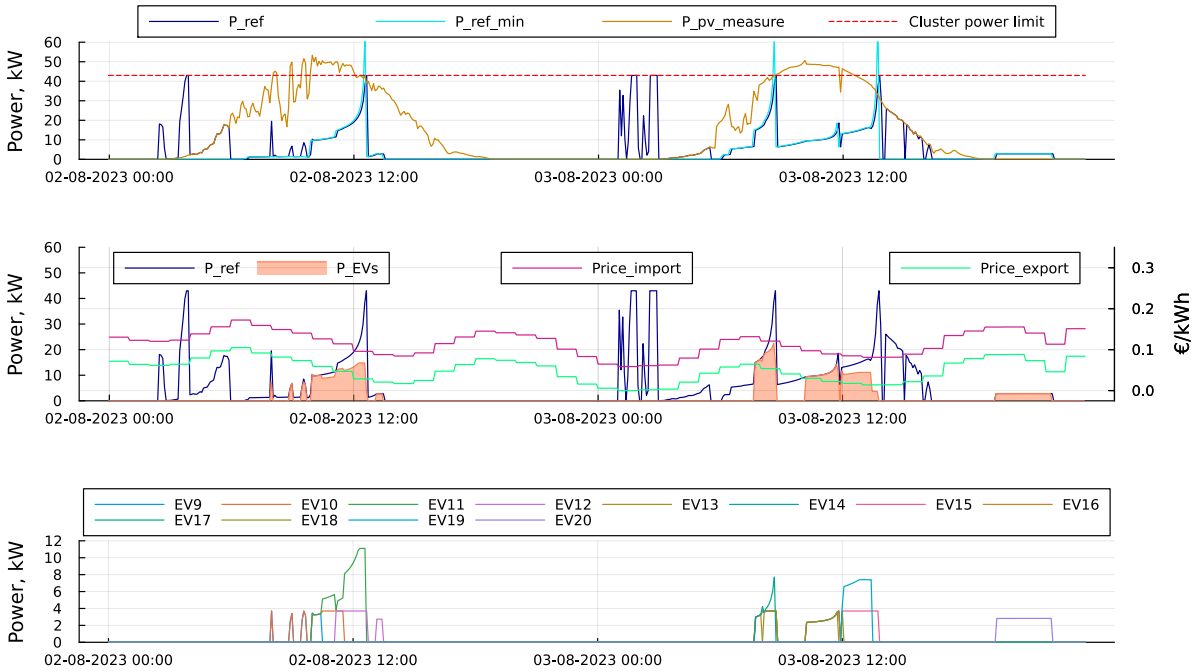

Figure 14: Summer case. Upper: Power reference allocated with P_ref_min, PV measurements and cluster limit; middle: power reference with electricity prices and aggregated power consumption of EVs; down: power consumption of each EV.

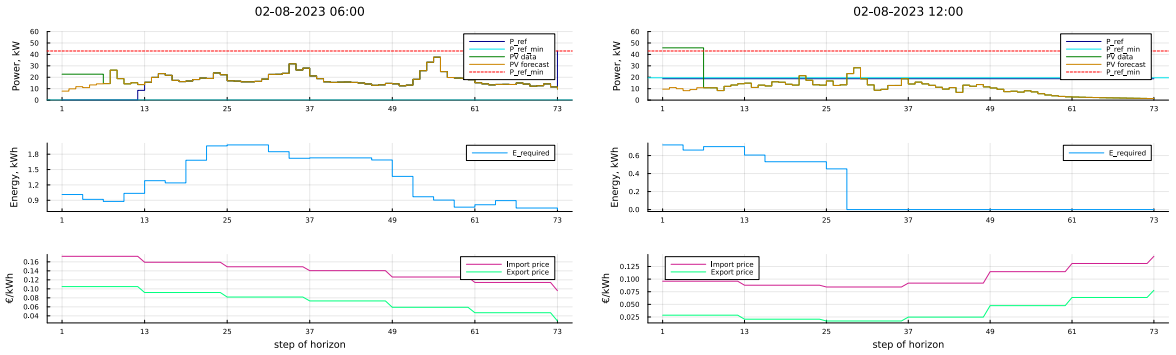

Figure 15: Power reference decision process outlook at 06:00 (left figure) and 12:00 (right figure) on 2nd of August 2023.

In the winter week, due to the low PV production in Denmark, the power reference is allocated based on prices and minimum power requests from the lower-level model, which is seen in Figure 8. The minimal PV production allows for only a small fraction of the EV consumption to be covered by local RES, which has been observed by previous demonstrations at the Danish location [9][10][11][12]. In the two displayed days for the winter week, the coincidence of the EV charging led to higher cluster consumption values compared to the summer case. Nevertheless, the control successfully kept the grid connection limit of 43 kW. More charging sessions are recorded on these two days of the winter week, as compared to Figure 14 from the summer week.

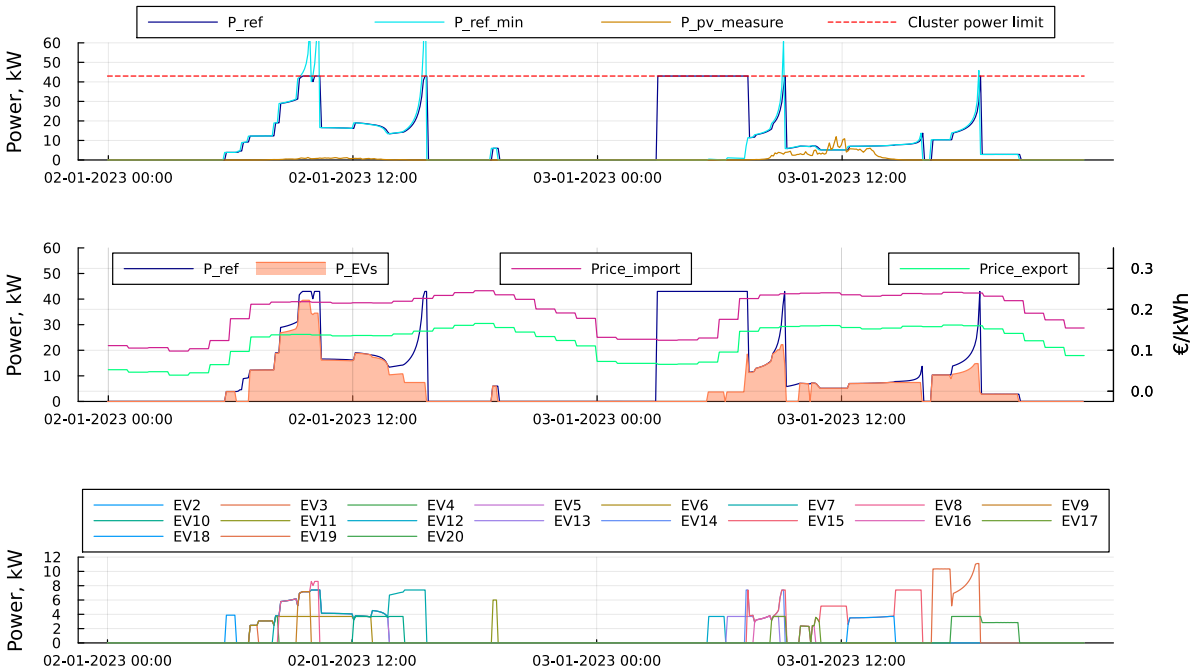

Figure 16: Winter case. Upper: Power reference allocated with P_ref_min, PV measurements and cluster limit; middle: power reference with electricity prices and aggregated power consumption of EVs; down: power consumption of each EV.

3.2.3.4 Scenarios comparison

Table 2 provides the assessment of scenarios for both summer and winter weeks. Firstly, the control model performed well with regards to the fulfillment of energy requests from EVs, considering that the allowed cluster power at 43kW is only one-third of the sum of the total installed charger power (132 kW). Also, it is noteworthy that under DSO command of power limitation for the cluster the energy request delivery is only 5-6% (summer and winter weeks) less compared to cluster limit and RES integration scenarios.

The economic assessment is conducted using several metrics. The electricity cost is the sum of electricity import expenses and export income. The electricity income only applies to the RES integration scenario as the research chargers are unidirectional and cannot export power. For the cluster limit and DSO command scenarios, the charging power is purely consumed from the grid and thus their import expenses are considerably higher compared to the RES integration scenario. Also, bared import expenses are higher in the winter week than in summer week as the electricity prices are higher in this period and EV consumption is higher with a larger number of charged EVs. The electricity export income from PV panel is much higher in the summer week than in the winter week as there is more excessive power generated by PV. Due to the same reason the summer week RES integration scenario is the only scenario when electricity cost is positive meaning income and not the expense.

For the total income of the charging station operator, the EV payments for charged energy are accounted for. The price is 0.34 € per kWh which is one of the lowest prices for charging energy in Denmark (value taken from charge point operator “Clever”). The total income is the sum of electricity cost and EV payment income. As seen from the table the total income in the RES integration scenario is higher than in any other scenario even in the winter week. Which proves the economic benefits of PV installation in the long run.

The last assessment is self-sufficiency and self-consumption for the RES integration case, based on [13]. Self-sufficiency defines the share of energy delivered to EVs from PV panel, while self-consumption defines the share of PV generated energy consumed locally by EVs. The high summer PV production allows the system to have self-sufficiency of 77% meaning that most of the charged energy is coming from PV. The 27% of self-consumption indicates that the system has extensive potential for consuming generation locally and allowing to have more consumption. However, the situation is flipped for the winter week as there is almost no excessive PV generation present in the system. Therefore, most of the energy charged to the EVs is coming from grid import power which is indicated by self-sufficiency of 13%. The majority of PV is consumed locally, with a self-consumption of 84%.

Table 2: Summer and winter assessment of all scenarios.

	Summer		
	Cluster limit	**DSO command**	**RES integration**
Delivery, %	91.3	86.1	91.9
Electricity cost (positive: income), €	-62.4	-59.3	36.2
Import expenses, €	-62.4	-59.3	-18.1
Export income, €	0.0	0.0	54.2
EVs payments income, €	214.0	201.9	215.3
Total income, €	151.6	142.6	251.5
Self-sufficiency, %	-	-	76.9
Self-consumption, %	-	-	27.3
	Winter		
	Cluster limit	**DSO command**	**RES integration**
Delivery, %	91.7	85.4	91.7
Electricity cost (positive – income), €	-181.8	-169.9	-156.0
Import expenses, €	-181.8	-169.9	-157.8
Export income, €	0.0	0.0	1.8
EVs payments income, €	331.4	308.9	331.4
Total income, €	149.6	139.0	175.4
Self-sufficiency, %	-	-	13.0
Self-consumption, %	-	-	84.3

3.3 Phase unbalance considerations

In case single-phase EVs are present in charging clusters, the charging processes can lead to phase unbalances. This phenomenon occurs when the distribution of loads across phases becomes uneven. To counteract this effect, load management systems could be designed to include load unbalance constraints in the decision making. This might even be required in cases where connection rules specify maximum values for phase imbalances.

In this section, an approach of including phase unbalance constraints in an optimization problem for EV load management systems is introduced and demonstrated through simulations. A nomenclature for the mathematical formulations is provided in Table 3.

Table 3: Nomenclature for cluster optimization with phase unbalance constraints.

Variables	Description
t	Set of time instances
b_i	Charging mode of EV i: 3 phase (1), 1 phase (0).
$E^{t}_{\mathrm{EV}_i}$	Charged energy of EV i.
$E^{\mathrm{re}}_{\mathrm{EV}_i}$	Requested energy of EV i.
k	Penalization costs for unfulfilled energy.
$P^{t}_{\mathrm{EV}_i}$	Three phase charging power of EV i at time t.
$P^{t}_{\mathrm{EV}i_1}$	Phase 1 charging power of EV i at time t.
$P^{t}_{\mathrm{EV}i_2}$	Phase 2 charging power of EV i at time t.
$P^{t}_{\mathrm{EV}i_3}$	Phase 3 charging power of EV i at time t.
$P^{\mathrm{EV}i_{per}}_{\mathrm{max}}$	Maximum single phase charging power of EV i.
$P^{\mathrm{EV}i_{per}}_{\mathrm{min}}$	Minimum single phase charging power of EV i.
$P^{t}_{\text{clu-A}}$	Phase A charging power of the cluster at time t.
$P^{t}_{\text{clu-B}}$	Phase B charging power of the cluster at time t.
$P^{t}_{\text{clu-C}}$	Phase C charging power of the cluster at time t.
$P^{ref-per}$	Power reference per phase of the cluster.
P^{t}_{clu}	Three phase charging power of the cluster at time t.
$P^{\mathrm{per}}_{\text{clu-maxdiff}}$	Maximum phase to phase power difference of the cluster.
α	Unfulfilled energy of the cluster at the end of optimization.
ψ_t	Energy price of the cluster.
$\gamma_{\mathrm{EV}i}$	Charging status of EV i: charging (1), not charging (0).

3.3.1 Methodology

The objective function of the optimization problem aims at minimizing the charging cost for the whole cluster while also making sure the energy requests of the drivers can be met, shown below:

$$\min \sum_{t} \left(P_{\text{clu}}^{t} \cdot \Delta t \cdot \psi_t \right) + k \cdot \alpha$$

where P_{clu}^{t} is the cluster charging power in three phases, Δt is the time step of each optimization cycle, ψ_t indicates the energy price of the cluster, α is the unfulfilled energy for the cluster, k is the corresponding penalty factor for the unfulfilled energy.

Constraints

Below are EV three phase power calculation constraints, where the charging power of each phase is limited to the range between the maximum and minimum allowed charging power.

$$P_{\text{min}}^{\text{EV}i_{per}} \cdot \gamma_{\text{EV}i} \leq P_{\text{EV}i_1}^{t} \leq P_{\text{max}}^{\text{EV}i_{per}} \cdot \gamma_{\text{EV}i}$$
$$P_{\text{min}}^{\text{EV}i_{per}} \cdot \gamma_{\text{EV}i} \leq P_{\text{EV}i_2}^{t} \leq P_{\text{max}}^{\text{EV}i_{per}} \cdot \gamma_{\text{EV}i}$$
$$P_{\text{min}}^{\text{EV}i_{per}} \cdot \gamma_{\text{EV}i} \leq P_{\text{EV}i_3}^{t} \leq P_{\text{max}}^{\text{EV}i_{per}} \cdot \gamma_{\text{EV}i}$$

where $\text{P}_{\text{min}}^{\text{EVi}_{per}}$ and $P_{\text{max}}^{\text{EV}i_{per}}$ are the minimum and maximum charging power of the EVi per phase, $\gamma_{\text{EV}i}$ is the charging status of the EV (1 for charging, 0 for not charging). If the EV is not charging, the charging power will be limited to 0 according to the constraints.

Cluster charging power constraints are presented to make sure that the cluster power of each phase is within the dedicated reference power range.

$$0 \leq P_{\text{clu-A}}^{t} \leq P^{ref-per}$$
$$0 \leq P_{\text{clu-B}}^{t} \leq P^{ref-per}$$
$$0 \leq P_{\text{clu-C}}^{t} \leq P^{ref-per}$$

Where $P_{\text{clu-A}}^{t}$, $P_{\text{clu-B}}^{t}$ and $P_{\text{clu-C}}^{t}$ are cluster charging power of each phase, $P^{ref-per}$ is the reference power on each phase.

The three-phase charging power of each EV is calculated by summing the charging power of each phase:

$$P_{\text{EV}i}^{t} = P_{\text{EV}i_1}^{t} \cdot \gamma_{\text{EV}i} + P_{\text{EV}i_2}^{t} \cdot \gamma_{\text{EV}i} + P_{\text{EV}i_3}^{t} \cdot \gamma_{\text{EV}i}$$

The charged energy of each EV is calculated by integrating the charging power multiplied with the specified time window:

$$E_{\text{EV}_i}^{t} = P_{\text{EV}_i}^{t} \cdot \Delta t + E_{\text{EV}_i}^{t-1}$$

The energy fulfilment constraint below requires the charged energy of each EV does not go above the requested energy. However, the cluster will be penalized if there is any gap between the charged energy and the requested energy, which makes sure that the energy goals are met eventually.

$$E^{t}_{\mathrm{EV}_i} \leq E^{\mathrm{re}}_{\mathrm{EV}_i}$$

The unfulfilled energy is calculated via deducting the overall charged energy from the collective requested energy of all participating EVs.

$$\alpha = \sum_{i} \mathrm{E}^{\mathrm{re}}_{\mathrm{EV_i}} - \sum_{i}\sum_{t} \left(\mathrm{P}^{\mathrm{t}}_{\mathrm{EV_i}} \cdot \Delta t\right)$$

The quantity α allows the cluster operator to penalize unfulfilled energy in the objective function, as described above.

Specific constraints are applied to single-phase EVs below, the charging power of phase 2 and phase 3 of each EV subjects to the charging mode.

$$P^{t}_{\mathrm{EV}i_2} = P^{t}_{\mathrm{EV}i_1} \cdot b_i$$
$$P^{t}_{\mathrm{EV}i_3} = P^{t}_{\mathrm{EV}i_1} \cdot b_i$$

Where $b_i$is a binary variable, indicating the charging mode of EVi. This shows that if an EV is a three-phase EV, then the charging power of phase 1, 2 and 3 should be equal, otherwise only phase 1 should have power.

Phase wiring is a setup that mix the phase connection between the plug and the cluster, shown in Figure 17. Since the single-phase EV only charges on the first phase of the plug, phase wiring is necessary to make sure that the cluster will not unbalance significantly if all connected EVs are single-phase EVs.

The charger phase combination implemented in the case study in the following section is: EV1 - ABC; EV2 - CAB; EV3 – BCA. Based on the combination, the cluster charging power per phase calculation is conducted by the constraints below:

$$P^{t}_{\text{clu-A}} = P^{t}_{\mathrm{EV}i_1} \cdot \gamma_{EVi} + P^{t}_{\mathrm{EV}(i+1)_2} \cdot \gamma_{EV(i+1)} + P^{t}_{\mathrm{EV}(i+2)_3} \cdot \gamma_{EV(i+2)}$$
$$P^{t}_{\text{clu-B}} = P^{t}_{\mathrm{EV}i_2} \cdot \gamma_{EVi} + P^{t}_{\mathrm{EV}(i+1)_3} \cdot \gamma_{EV(i+1)} + P^{t}_{\mathrm{EV}(i+2)_1} \cdot \gamma_{EV(i+2)}$$
$$P^{t}_{\text{clu-C}} = P^{t}_{\mathrm{EV}i_3} \cdot \gamma_{EVi} + P^{t}_{\mathrm{EV}(i+1)_1} \cdot \gamma_{EV(i+1)} + P^{t}_{\mathrm{EV}(i+2)_2} \cdot \gamma_{EV(i+2)}$$

The cluster charging power in three phases is calculated by summing the single-phase cluster charging power:

$$P^{t}_{\mathrm{clu}} = P^{t}_{\text{clu-A}} + P^{t}_{\text{clu-B}} + P^{t}_{\text{clu-C}}$$

The cluster charging power unbalance constraints make sure that the power difference between any two phases is within the pre-set limit:

$$-P^{\mathrm{per}}_{\text{clu-maxdiff}} \leq P^{t}_{\text{clu-A}} - P^{t}_{\text{clu-B}} \leq P^{\mathrm{per}}_{\text{clu-maxdiff}}$$
$$-P^{\mathrm{per}}_{\text{clu-maxdiff}} \leq P^{t}_{\text{clu-A}} - P^{t}_{\text{clu-C}} \leq P^{\mathrm{per}}_{\text{clu-maxdiff}}$$
$$-P^{\mathrm{per}}_{\text{clu-maxdiff}} \leq P^{t}_{\text{clu-B}} - P^{t}_{\text{clu-C}} \leq P^{\mathrm{per}}_{\text{clu-maxdiff}}$$

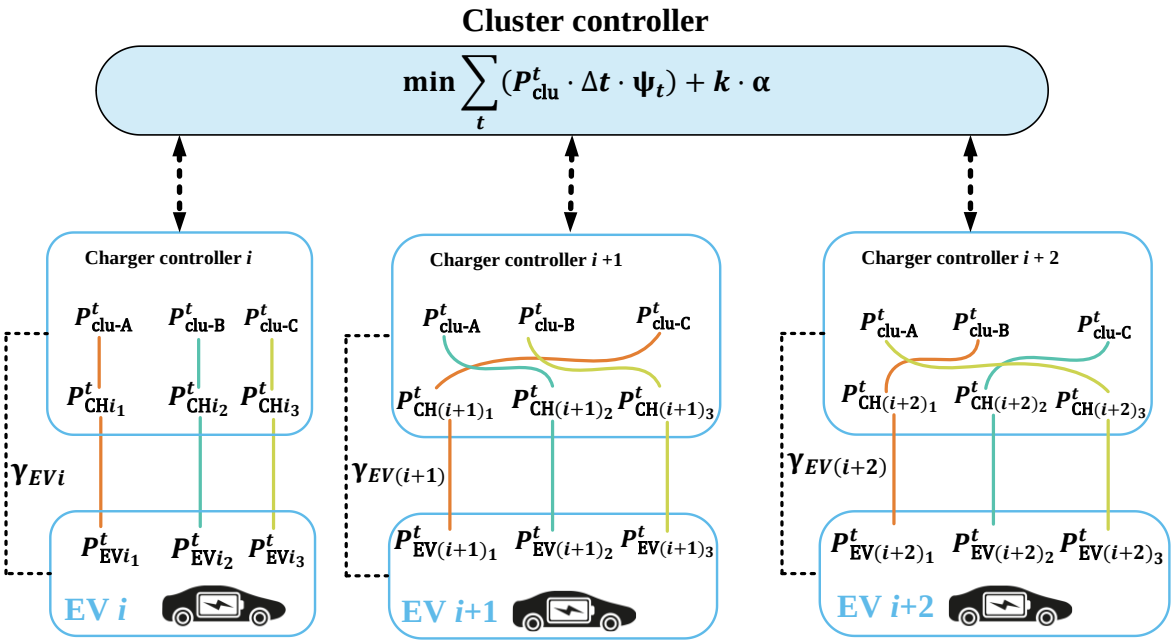

Figure 17: Charging cluster layout – phase wiring is implemented to mix the phase connection between each plug and the cluster.

3.3.2 Simulation scenario

A simulation is conducted to test the functionality of the optimization method introduced above. Three EVs are tested, where the information is shown in Table 4. EV2 and EV3 are selected as single-phase EV to make sure the occurrence of phase unbalance events without load management. Since a single-phase EV only charges in the first phase of the plug, and phase wiring in plug configuration is implemented according to Figure 17, EV2 and EV3 will then charge in phase C and phase B respectively.

Table 4: Overview of simulation parameters for phase unbalance considerations.

EV	Charging type	Requested energy	Phase wiring configuration	Maximum power per phase	Minimum power per phase
EV1	Three-phase	30 kWh	ABC	3.68 kW	1.38 kW
EV2	single-phase	20 kWh	CAB	3.68 kW	1.38 kW
EV3	single-phase	18 kWh	BCA	3.68 kW	1.38 kW

The cluster power reference for three EVs is set to 22 kW in three phases, each plug provides maximum charging power of 11 kW in three phases. The penalty factor k is set to 0.5 €/kWh, which indicates that every unfulfilled kWh causes 0.5 € of additional cost. The simulation time is set to 10 hours, with the time step of 1 hour. All EVs are connected during the simulation. The electricity price starts from 0.30 €/kWh at the beginning and linearly increases to 0.48 €/kWh in the end with a step of 0.02 €/kWh for each hour slot.

3.3.3 Results and discussion

This subsection summarizes the simulation results for testing the optimization model with phase unbalance constraints. Figure 18 shows the charging profile when there is no phase power difference limitation considered in the optimization problem. The top figure shows the charging power in three phases of each EV, and the bottom figure presents the phase power of the whole charging cluster. Since the energy price increases progressively according to the charging time, the controller tries to schedule charging sessions as early as possible to minimize the cost. The maximum phase power difference occurs in the first three hours, reaching 3.67 kW. All charging sessions finish at the sixth hour. The energy cost for the whole cluster is 22.5 € in the end.

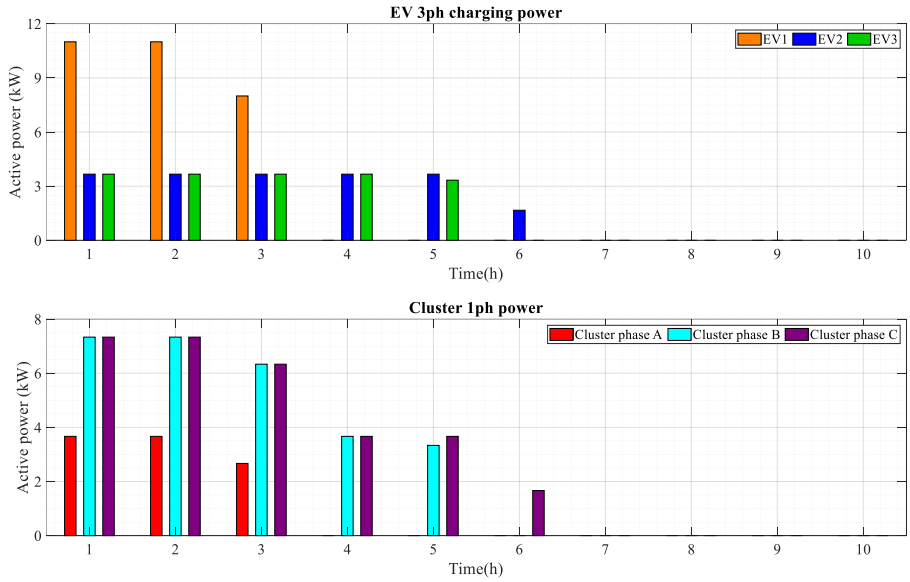

Figure 18: Charging profile of the cluster and the EVs without phase power difference limitation.

Figure 19 shows the charging profile when the maximum phase power difference is limited to 2 kW in the optimization problem. Therefore, the maximum phase power difference occurring in the first three hours is then constrained to 2 kW. The limited phase power difference stems from the reduction of charging power for EV2 and EV3, as a result, the charging time is extended to the nineth hour for EV3 and tenth hour for EV2 to meet their energy goals. Since more charging sessions are scheduled later with higher energy prices, the energy cost for the whole cluster increases to 24.2 €.

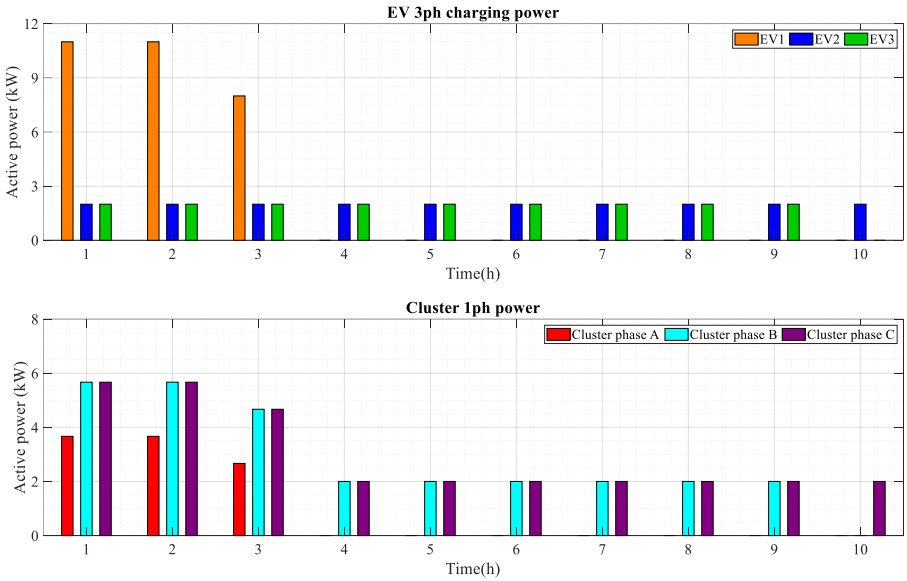

Figure 19: Charging profile of the cluster and the EVs with 2 kW phase power difference maximum.

In general, in the situations where a significant amount of single-phase EVs need to be charged in the cluster, the phase-to-phase power difference could lead to an unbalance issue in the distribution system. While the phase power constraints in the optimization manage to keep the unbalance within a preset range, the energy goal needs to be fulfilled with an extended period. Such trade-off may also be integrated in the smart charging management algorithm with other control purposes. The experimental validation is planned in DTU Risø campus in the forthcoming months, as part of WP9. Additionally, [16] will apply historical charging profile data to validate the functionality of the proposed method.

3.4 Frequency control

In the present section, the technical capability of EV charging infrastructure to provide frequency control as a service to TSOs is assessed. The work is based on [14] and develops a distributed control method utilizing the autonomous controllability of the chargers deployed in the Danish demonstration. The control model is implemented in Matlab Simulink and the model parameters are adapted to the physical characteristics of the demonstration cluster. Finally, the simulation results with the distributed control are compared to the ones with a centralized control model. A nomenclature for the mathematical formulations and figures in this section is provided in Table 5.

Table 5: Nomenclature for frequency control.

Variables	Description
d_{AWS}	Amazon Web Services delay
$d_{Energidata}$	Energidata.dk delay
d_{WB}	Whiteboard delay
$E_{charged}$	Energy supplied to an EV during a charging session
E_{req}	Energy requested by the user during a charging session
f_{grid}	Grid frequency measured at the PCC
f_{nom}	Nominal grid frequency
f_{range}	Frequency range where the droop control is active
$P^{t}_{ref,k}$	Power reference from the VA to EV *k* at time *t*
$P^{t}_{error,PCC}$	Power error at the PCC at time *t*
P_{bid}	Bid power
P_{max}	Upper power limit
P_{min}	Lower power limit
t_{charge}	Charging time requested by the user
t_{dep}	Departure time
t_{now}	Arrival time
TS^{write}_{CA}	Writing time stamp of Cloud Aggregator on WB
$TS^{variation}_{EV\ current}$	Time stamp of EV current measurement variation
$TS^{variation}_{PWM}$	Time stamp of PWM signal variation
TS^{write}_{VA}	Writing time stamp of Virtual Aggregator on WB
$TS^{read}_{WBlogger}$	Reading time stamp of WBlogger function from WB
$\rho_{abs,k}$	Abs. priority computed by the *k*-th VA and broadcasted to other VAs
$\rho_{rel,k}$	Rel. priority comp. by the *k*-th VA considering abs. priorities from all VAs

3.4.1 Methodology

Each of the chargers deployed in the Danish demonstration are equipped with a local controller that enables the charger to make autonomous control decisions. This facilitates distributed control schemes where all chargers are provided with global quantities, such as the cluster reference power

and the actual cluster consumption, based on which all chargers individually control their respective charging session to collectively meet the cluster requirements. This control method promises various benefits, such as a fast response time, reduced data traffic and higher data security, as well as a reduced risk of single point failure, as opposed to centralized management systems. A preliminary demonstration of the charger functionalities was presented in [17][18].

3.4.1.1 Control architecture

The actual implementation of the control architecture employed in the Danish demonstration has been previously described in [1], and comprises two different control entities. The Cloud Aggregator (CA) provides a global reference value for the cluster consumption, while the different Virtual Aggregators (VA) – one per charger – calculate the individual reference power for each charger locally.

To assess the capability of the distributed control method to provide frequency control, a simulation model was developed. Figure 20 provides a high-level overview of the control model. The CA calculates the cluster power reference based on a local measurement of the system frequency. This cluster reference is communicated to the VAs, who calculate the difference between the reference and the measurement at the PCC – defined as the power error. This power error is fed into the priority system of the VA, which calculates what share of the power difference should be covered by the own charger, based on the own urgency of charging. The priority system has been previously introduced in [18]. It calculates the priority based on the EVs energy request and prospective charging time and normalizes it using the priorities of the other EVs. Based on its priority, the VA provides a setpoint to the EV via the Pulse-Width Modulation (PWM) signal of the AC charging cable. The compliance and reaction time of the EV with this setpoint is calculated in the EV model.

In a centralized control system, the same control decisions are performed, however, by a single entity. The results are then communicated to the chargers, which will convert the setpoint to a PWM signal for the EV. One aspect that is worth noticing, is the fact that with the distributed configuration the measurement loop is shorter (i.e., the PCC power is directly provided to the VAs), and thus also the response time for the system is expected to be smaller.

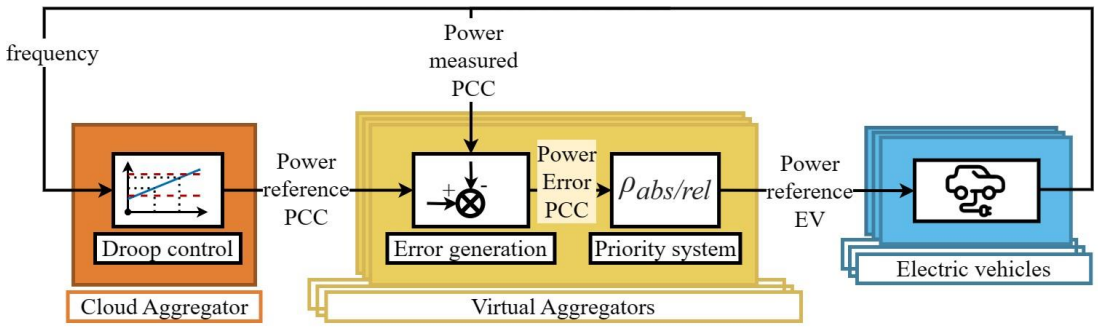

Figure 20: High level control diagram for the distributed system providing frequency control.

The control system was modeled in Matlab Simulink®. In the following, the different elements in the model are presented. First, the modelling of the CA and VAs is presented, then the modelling of the

different communication and reaction delays present in the system (Whiteboard, Amazon Web Services, Energidata.dk and the EVs).

3.4.1.2 Cloud aggregator and virtual aggregator

The CA and the VAs are represented in Simulink as triggered subsystems. Thus, the functions (blocks) placed inside them are run every time the subsystem is triggered. This is done to represent the fact that these elements do not run continuously, but in a discrete manner. The Update Rate (UR) of the CA and VAs are critical values, and they should be properly tuned in order to obtain a stable control system. The subsystems are triggered by an external signal through a trigger port, whenever it transitions to a specified direction. The direction can be rising, falling or either rising or falling. A rising transition occurs when the signal changes from a negative value to either zero or a positive value, while a falling transition happens when the signal changes from a positive value to either zero or a negative value. In the present model, the subsystem is set to trigger to a rising signal, and the trigger signal is provided by a square wave generator block. By adjusting the frequency parameter inside the square wave generator block, it is possible to generate a triggering signal with different frequencies, and therefore to change the UR of the CA and VAs.

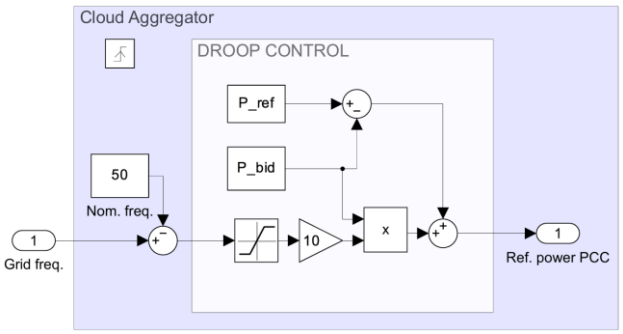

Figure 21: Implementation of the cloud aggregator model in Matlab Simulink.

The Simulink implementation of the CA is shown in Figure 21. To perform the droop control, the grid frequency f_{grid} (measured by the meter) is compared with the nominal frequency f_{nom} (equal to 50 Hz). The frequency regulation happens between 49.9 and 50.1 Hz, therefore the frequency deviation is then saturated between -0.1 and +0.1 Hz. The saturated error is multiplied by 10, and then used to compute the percentage of bid power P_{bid} to add/subtract to the amount of $P_{ref} - P_{bid}$, where P_{ref} is the maximum cluster power. The resulting power is the reference power, the output of the droop control function. For more information regarding the provision of frequency control in the Nordic synchronous area, the interested reader is referred to [19][20].

The virtual aggregators are also modelled as triggered subsystem, as shown in Figure 22. The VA calculates the error in the power output using the measurement at the PCC, as seen on the leftmost of the figure.

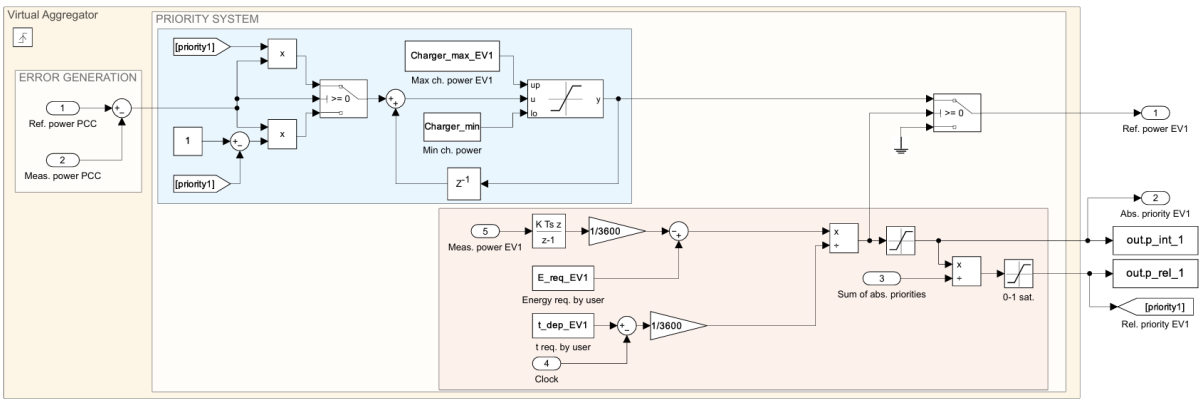

Figure 22: Implementation of the virtual aggregator model in Matlab Simulink.

The priority system is performed through a switch block, and the power error at the PCC is multiplied by ρ_{rel} when the error is positive and by $(1-\rho_{rel})$ when the error is negative, according to the following equation:

$$P^{t}_{ref,k} = \begin{cases} P^{t-1}_{ref,k} + P^{t}_{error,PCC} \cdot \rho_{rel,k} & when\ P^{t}_{error,PCC} > 0 \\ P^{t-1}_{ref,k} + P^{t}_{error,PCC} \cdot (1-\rho_{rel,k}) & when\ P^{t}_{error,PCC} < 0. \end{cases}$$

The relative priorities are computed starting from the user's information and exploiting the absolute priorities shared by the other VAs, as described by the following equations:

$$\rho_{abs} = \frac{E_{req} - E_{charged}}{t_{dep} - t_{now}}$$

$$\rho_{rel,k} = \frac{\rho_{abs,k}}{\sum_{i=1}^{N^\circ EVs} \rho_{abs,i}},$$

where E_{req} is the energy requested by the user, $E_{charged}$ is the energy already provided to the user, estimated at each step from the measured power and t_{dep} and t_{now} are respectively the departure and arrival times, which are set by the user.

The portion of the PCC error, after going through the priority system function is then added to the charging power at the previous timestep. This is implemented in Simulink through a delay block, imposing a delay length of one timestep. The control method presented in Figure 22 considers that the charging power capability depends on the respective EV model, as well as factors such as the vehicle State of Charge (SOC) and the temperature [21][22][23]. The system ensures that the available cluster power is utilized by EVs with lower priority, in case EVs with higher priority cannot increase their charging power further.

3.4.1.3 Delays for Whiteboard, AWS, Energidata.dk, and EV

The analyzed system is characterized by different communication delays, related to the transmission of data (WB, AWS, Energidata.dk), and by reaction delays, related to the reception of commands (EV reaction time). As previously introduced in [1], the two main channels of communication in the Danish demonstration are the custom-made Whiteboard (WB) and the Amazon Web Services (AWS). These solutions are used to store and retrieve the last communication set points. AWS is responsible for the

communication between the VAs and the charger actuators, while WB is the local shared data storage responsible for the communication between all the control components.

The communication delays are modelled in Simulink employing the Transport Delay block. This block needs two essential parameters, to correctly model the system: the time delay parameter, representing the amount of time it takes for information to propagate from the input to the output of the block, and the initial output, which specifies the initial condition of the output signal when the simulation starts. It is essential to set this parameter correctly to ensure that the system behaves as expected from the beginning of the simulation. The values for these parameters have been evaluated in laboratory tests, which are described in the next section. The WB delay and the AWS delays have been modelled only with this block. The Energidata.dk delay, modelling the communication delay between the meter and the CA/VAs, has instead been modelled as a Transport Delay block in series with a subsystem which is triggered every one second, modelling the fact that the meter reads the measures every one second. The three communication delays, modelled in Simulink, are shown in Figure 23.

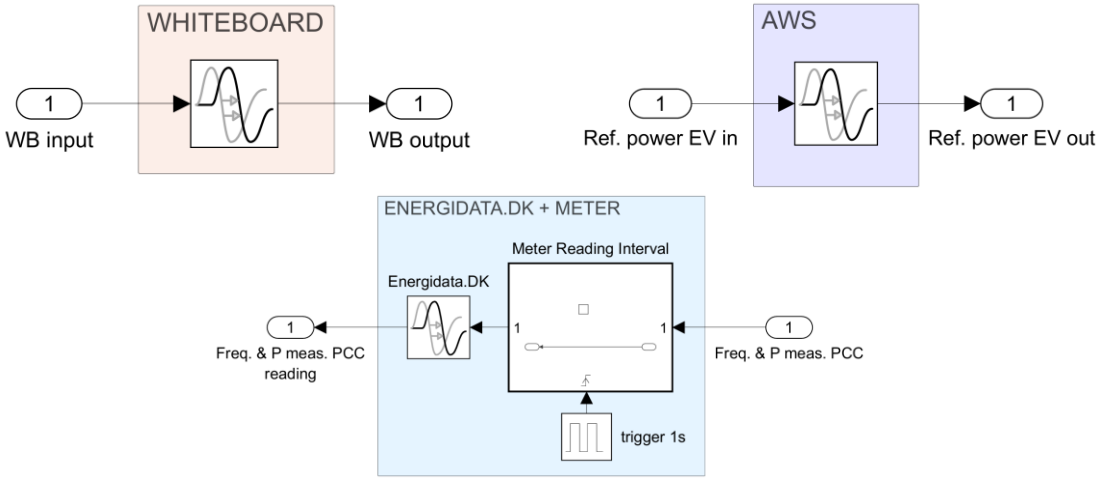

Figure 23: Implementation of delays in Matlab Simulink.

The charger provides the EV with the maximum allowed charging power, through a PWM signal. The EV receives the variation in the PWM signal through the CP pin and needs some time to change its power absorption. According to paper [15], the delayed response can be split into two subsequent behaviours: a delayed reaction, followed by a limited slope for the power variation. A typical EV response to a variation in the maximum allowed current is shown in Figure 24.

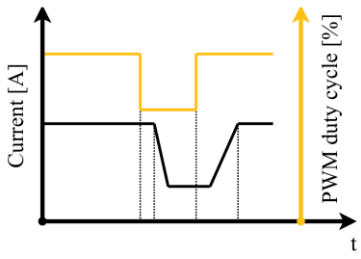

Figure 24: Response delay of EV to a change in the charger setpoint.

These two parameters depend on the EV model, and also on the derivative of the power reference (increasing or decreasing). Usually, if the power reference is decreasing the overall response is faster, since the reaction time is smaller and the power decreases more rapidly. The presented system is modelled in Simulink in the way shown in Figure 25.

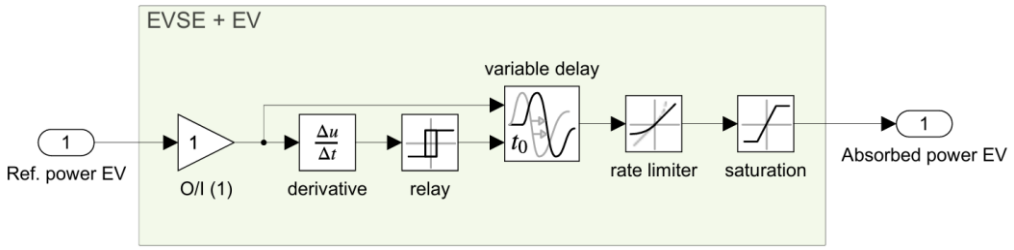

Figure 25: Implementation of EV response delay in Matlab Simulink.

Starting from the left, a derivative block is present, to detect whether the power reference is increasing or decreasing. Depending on the sign of the derivative, the relay block can then output two different delay values which are provided to the variable delay block. The variable delay block takes the power reference and delays it by an amount equal to the one provided by the relay block. The delayed power is then provided to a rate limiter block. The rate limiter block has also two values for the maximum rate, depending on whether the input value is increasing or decreasing. At last, a saturation block is used to represent the power absorption limits of the EV. This is an important parameter since it is possible that the EV is not always able to charge at the maximum allowed power, due to the SOC level, or to critical external conditions. Currently, however, the power individually absorbed by each vehicle is only used to compute the energy $E_{charged}$ provided to the EV during the charging session and a system to detect potential EV saturation has not yet been implemented.

As described in the previous section, the model presents some parameters which need to be properly determined, to make sure that the model behaves as similarly as possible to the real system. These parameters are the following (individual delays):

Whiteboard delay: d_{WB}

It is defined as the time necessary for the complete process of uploading and downloading to and from Whiteboard. It is estimated utilizing an additional Python script called WB logger, which continuously reads Whiteboard, waiting for a change in the power reference from the CA. The CA records on a .csv file the sending Time Stamp (TS) of the reference signal, and the WB logger function records on another .csv file the reading time stamp from WB. Therefore, it can be computed as:

$$d_{WB} = TS^{read}_{WBlogger} - TS^{write}_{CA}.$$

Amazon Web Service delay: d_{AWS}

The Amazon Web Service delay is estimated by recording the sending time of the setpoint by the VA, recorded in a .csv file, and the time of the subsequent variation in the PWM duty cycle of the charger, recorded in another .csv file by a Python script. The duty cycle is measured using a clamp meter, positioned around the Control Pilot cable. The AWS delay can thus be expressed as:

$$d_{AWS} = TS^{variation}_{PWM} - TS^{write}_{VA}.$$

Energidata.dk delay: $d_{Energidata}$

The Energidata.dk delay is measured by comparing the times tamp of the variation in the EV charging current, which is measured by another clamp around one phase of the EV charging cables, and the time stamp of the variation in the reading of the current measurement, as seen by the WB logger function. The Energidata.dk delay can thus be computed as:

$$d_{\text{Energidata}} = TS^{\text{read}}_{\text{WBlogger}} - TS^{\text{variation}}_{\text{EV current}}.$$

Therefore, $d_{Energidata}$ includes the time needed for the meter to upload the measure on the Energidata platform, for the transfer of the measure onto Whiteboard, and finally for reading the Whiteboard data. As previously seen, the meter has a sampling period of 1 s. Therefore, the measured delay will be, on average, higher than the effective one by 0.5 seconds.

3.4.1.4 Quantification of model parameters

Since the deployment of the charging infrastructure at Risø is already well advanced, the various control and response delays were quantified with the available hardware & software components. This allows for the realistic implementation and testing of control methods in the simulation model. For the characterization of the delays, the propagation of the control signals from an initial setpoint change to the response of the EV was observed. The results are presented in Figure 26 and Figure 27.

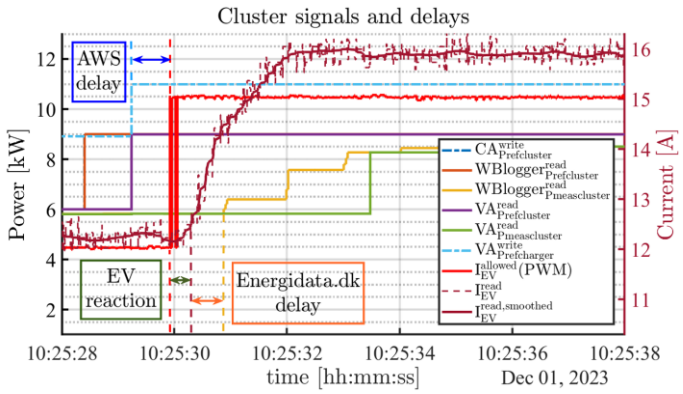

Figure 26: Quantification of the signal delays in the Risø charging cluster.

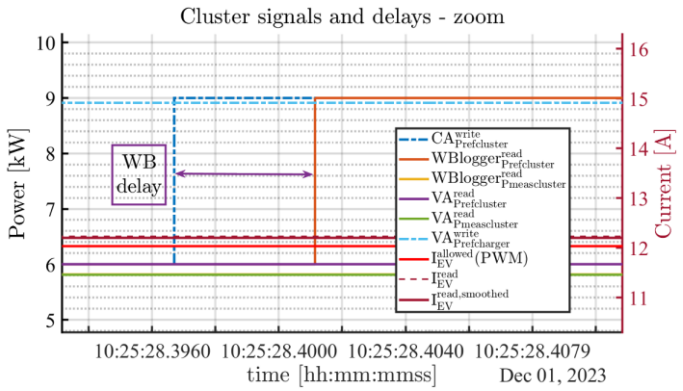

Figure 27: Excerpt of the recorded signal delays in the Risø charging cluster.

Based on the measurements, the following average delays were determined:

- $d_{WB} = 0.00$ s
- $d_{AWS} = 1.39$ s
- $d_{Energidata} = 1.06$ s

The averages of the three individual delays are then used in the Simulink model, inside the respective blocks.

3.4.2 Comparison of centralized and distributed control

The technical capability of the distributed control architecture is tested using the simulation model introduced above. Moreover, the simulation results are compared to the centralized control.

3.4.2.1 Model inputs

In the simulation, a cluster composed of two EVs is considered. To correctly set the simulation it is necessary to provide the control system with information regarding the power limits for the PCC, the frequency range in which regulation takes place, the maximum and minimum admitted power for each EV, the charging time, and the energy required for the charging session. The information relative to the PCC is reported in Table 6, while information regarding the EVs is reported in Table 7.

Table 6: PCC model inputs

	PCC
P_{min}	13 kW
P_{max}	19 kW
f_{range}	49.9 – 50.1 Hz

Table 7: Model inputs for EVs

	EV1	EV2
Model	Renault Zoe 40	
P_{min}	6 kW	3.55 kW
P_{max}	9.3 kW	9 kW
t_{charge}	3 h	3 h
E_{req}	19 kWh	8 kWh

Exploiting the absolute priority definition, it is possible to compute the initial average charging power needed for the two EVs to acquire the requested energy E_{req} in the requested time t_{charge}. By exploiting the relative priority definition, relative priorities are computed. These initial priorities are reported in Table 8.

Table 8: EV priorities for the simulation

	EV1	EV2
Absolute priority ρ_{abs}	6.3 kW	2.7 kW
Relative priority ρ_{abs}	0.7	0.3

According to the relative priorities, in the initial phase of the test the first EV will absorb 70% of the error at the PCC, while the second EV will cover 30% of the error at the PCC. At each iteration, each VA computes the acquired energy by integration of the measured power at the plug. Thus, the absolute

priority ρ_{abs} is updated according to the absolute priority definition, and a new value is uploaded on Whiteboard. From there, the other EV reads the value, and computes its own relative priority ρ_{rel}. For this reason, the share of error at PCC which each EV takes changes at each iteration and should decrease as the EV approaches the required energy faster than the other EVs.

3.4.2.2 Simulation results

Figure 28 compares the power reference at the PCC (P reference PCC) with the actual power absorbed by the cluster at the PCC (P measured PCC). The absorbed power is delayed with respect to the reference, as expected, due to communication delays, and due to the EVs reaction time.

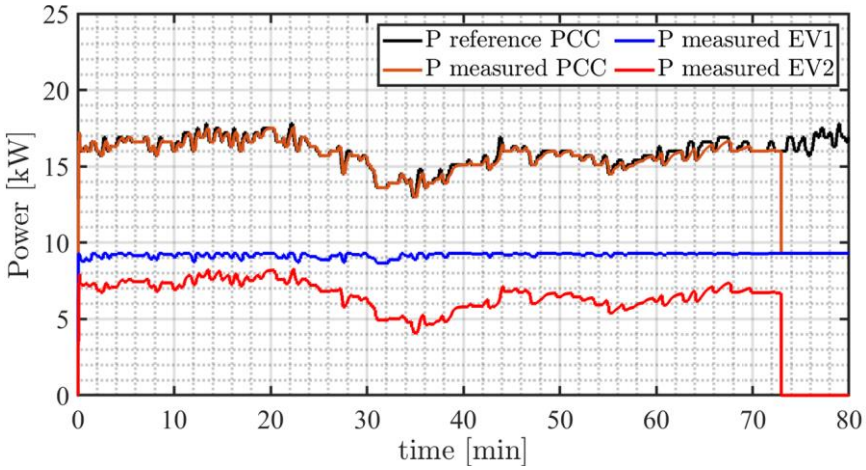

Figure 28: Simulation result for frequency control model with distributed control architecture.

When observing the power of both EVs, it is apparent that the EV1 is in saturation condition, i.e., it reaches its maximum power. This is due to the power repartition, based on the priority system. EV1 has, in fact, a higher priority with respect to EV2, resulting in a larger proportion of the available reference power.

To compare the distributed architecture with the centralized one, the simulation was also run using the centralized architecture, applying the same parameters as for the distributed architecture. The main consequence of this consists in the feedback loop being larger since the measurement from the PCC is sent first to the CA and from there, the control signal is sent to the VAs. Due to the higher feedback delay, the UR of the VAs in the centralized configuration cannot be as high as the UR of the VAs in the distributed configuration. If the UR of the VAs is too high, each VA will update more than once before the effect of its actions on the PCC measurements is registered by the same VA, which may cause an over- or undershoot of the aggregated EV response. This behavior can be observed in Figure 29, where the output from the centralized model is compared with the output from the distributed model. To provide a clearer picture, the plot shows a representative time window of the simulation result previously presented in Figure 28.

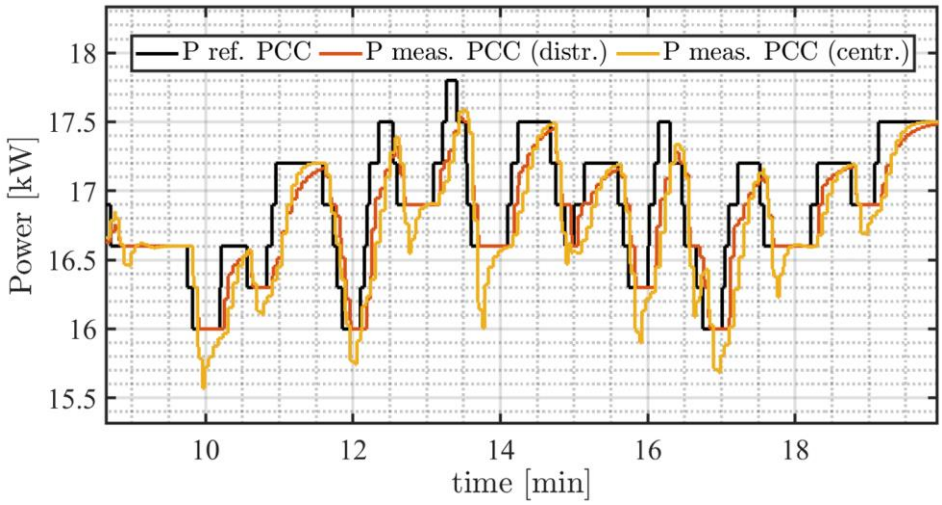

Figure 29: Comparison of frequency control provided by distributed and centralized control architecture.

It is noticeable that the centralized architecture is more unstable, especially in the downward direction. This is because EV1 is saturated in the upper direction, and therefore the overshooting in this direction is compensated by the absence of power provided by EV1. On the contrary, in the lower direction, the cluster reacts with all the EVs, but the fast UR of the VAs causes undershooting.

The simulations allowed for a quantification of the average response time for both architectures. With the distributed control, the average response time between frequency deviation and aggregated EV response was 7.27 s, and with the centralized control 7.97 s. Hence, the distributed control is on average around 9% faster than the centralized control. Moreover, as previously mentioned, the shorter control loops make the distributed control more stable in its response, with the reference value followed more closely.

4 Conclusions

This deliverable presents the modelling framework and research backbone to the development of V2X strategies for the demonstration activities in Denmark described in WP9. The charging infrastructure at the Danish demos comprises twelve AC charge points with a rated power of 11kW each. The cluster management system serves two main purposes. Firstly, it ensures the compliance with grid connection limits, as the PCC power rating of 43 kW is lower than the sum of the rated power of all chargers of 132 kW. Secondly, it utilizes the flexibility of charging processes to provide services both behind and in front of the meter. The modelling framework comprised forecast models to predict the EV charging demand (consumption side), and the expected generation from a local PV system (production side). These forecast models were integrated in the control models developed within the scope of this work. Moreover, EV users at the Danish demo sites can provide their estimated departure time and energy needs through an app, which is taken into account in the decision-making process.

The control models facilitated the coordination of EV charging for providing services to local and external grids and were tested in different scenarios, using actual PV production and EV charging data from both winter and summer weeks. It was shown that the control complies with local grid connection limits and is able to provide demand response to DSOs by reducing the cluster power limit on request. The tested reduction of the cluster by half from 43 kW to 21.5 kW on weekdays between 7 a.m. and 12 p.m. led to a decrease of the fulfilled energy requested by the EVs by 5% in the summer scenario and 6% in the winter scenario. Yet, this decrease is small considering that the power reduction was requested for 5 consecutive hours with frequent EV arrivals.

The consideration of local PV generation, as present at the Danish demo site Campus Bornholm, incentivized the control to prioritize times that allow using PV energy to meet the local EV demand. In the summer scenario, an overall proportion of 77% of the energy delivered to EVs was provided by the local PV system, defining the system's self-sufficiency. Conversely, 27% of the total energy provided by the local PV system was utilized for EV charging, defining the system's self-consumption. In the winter scenario, the values for self-sufficiency and self-consumption were 13% and 84%, respectively.

Additionally, an approach for including phase unbalance constraints in an optimization problem formulation for EV load management systems was introduced and demonstrated through simulations. It was shown how charging processes of single-phase EVs can lead to unbalances between the three phases of the cluster. Load management systems with phase unbalance constraints can counteract this effect at the cost of longer charging times for single-phase EVs.

Finally, the technical capability of EV charging infrastructure to provide frequency control was assessed. The work investigated a distributed control method utilizing the autonomous controllability of the chargers deployed in the Danish demonstration. The model parameters, such as delays from hardware and software, were characterized through the installation at Risø Campus. The simulation results showed that the distributed control architecture enables a 9% faster response compared to the centralized method and followed the reference value more closely.

The developed control methods serve as a basis for the upcoming demonstrations in WP9. In this regard, the experimental testing is expected to provide important insights on how the proposed methods perform within real operational settings.

References

[1] Engelhardt et al., “Deliverable D9.1: Use case specification, development, installation, commissioning, demonstration, and evaluation planning for the Danish demo”, 2023.

[2] Ziras et al., “Deliverable D2.2 Control strategies for V2X integration in buildings,” 2023.

[3] Mateus et al., “Deliverable D2.1 Control Strategies for V2X Integration in Houses,” 2023.

[4] LIGHTGBM. Welcome to LightGBM’s documentation! - LightGBM 4.0.0 documentation. (n.d.). https://lightgbm.readthedocs.io/en/stable/

[5] X. Yao, X. Fu, and C. Zong. "Short-term load forecasting method based on feature preference strategy and LightGBM-XGboost." IEEE Access 10 (2022): 75257-75268.

[6] Shcherbakov, Maxim Vladimirovich, et al. "A survey of forecast error measures." World applied sciences journal 24.24 (2013): 171-176.

[7] A. Malkova et al., “Receding horizon optimization for workplace electric vehicle charging station with PV panel coordination”, 2024, in preparation.

[8] A. Malkova; J. M. Zepter, and M. Marinelli. “Online optimization of a workplace electric vehicle charging station under grid constraints.” 2023. Paper presented at 7th E-Mobility Power System Integration Symposium, Lyngby, Denmark.

[9] J. Engelhardt, J. M. Zepter, T. Gabderakhmanova, and M. Marinelli, "Energy Management of a Multi-Battery System for Renewable-Based High Power EV Charging," In: eTransportation, 2022.

[10] J. Engelhardt, "Reconfigurable Batteries in Electric Vehicle Fast Chargers: Towards Renewable-Powered Mobility," DTU Wind and Energy Systems, 2022.

[11] A. Bowen, J. Engelhardt, T. Gabderakhmanova, M. Marinelli, and G. Rohde, "Battery Buffered EV Fast Chargers on Bornholm: Charging Patterns and Grid Integration," in Proceedings of the 57th International Universities Power Engineering Conference (UPEC), Istanbul, Turkey, 2022.

[12] J. Engelhardt, J. M. Zepter, J. P. Sparresø, and M. Marinelli, "Real-life demonstration of a hybrid EV fast charging station with reconfigurable battery technology enabling renewable-powered mobility," in Proceedings of the 18th Conference on Sustainable Development of Energy, Water, and Environment Systems (SDEWES), Dubrovnik, Croatia, 2023.

[13] J. M. Zepter, J. Engelhardt, T. Gabderakhmanova, and M. Marinelli, "Re-Thinking the Definition of Self-Sufficiency in Systems with Energy Storage," in Proceedings of the 2022 International Conference on Smart Energy Systems and Technologies (SEST), IEEE, pp. 1–6.

[14] P. Zunino, “Analysis and testing of frequency services provided by electric vehicle clusters”, 2024, Master thesis.

[15] Sevdari, K., Andersen, P. B. & Marinelli, M. “Aggregation and control of electric vehicle AC charging for grid services”, 2023, submitted to: IEEE Transactions on Smart Grid (under review)

[16] X. Cao et al. “Load management for EV cluster charging considering phase unbalance constraints”, 2024, in preparation.

[17] X. Cao, S. Striani, J. Engelhard, C. Ziras and M. Marinelli. “A semi-distributed charging strategy for electric vehicle clusters”. Energy Reports. 2023.

[18] X. Cao, J. Engelhardt, C. Ziras and M. Marinelli. “Distributed control of electric vehicle clusters for user-based power scheduling”. In Proceedings of 2023 IEEE Transportation Electrification Conference and Expo, Asia-Pacific (ITEC-AP 2023). IEEE. 2024.

[19] J. Engelhardt, A. Thingvad, J. M. Zepter, T. Gabderakhmanova, and M. Marinelli, "Energy Recovery Strategies for Batteries Providing Frequency Containment Reserve in the Nordic Power System," Sustainable Energy, Grids and Networks, vol. 32, p. 100947, 2022.

[20] A. Thingvad, C. Ziras, G. Le Ray, J. Engelhardt, R. Mosbæk, and M. Marinelli, "Economic Value of Multi-Market Bidding in Nordic Frequency Markets," in Proceedings of International Conference on Renewable Energies and Smart Technologies, IEEE, 2022.

[21]J. Engelhardt, S. Grillo, L. Calearo, M. Agostini, M. Coppo, and M. Marinelli, “Optimal control of a DC microgrid with busbar matrix for high power EV charging,” Electric Power Systems Research, vol. 224, p. 109680, 2023.
[22]M. Marinelli, L. Calearo, and J. Engelhardt, "A Simplified Electric Vehicle Battery Degradation Model Validated with the Nissan LEAF e-plus 62-kWh," in Proceedings of 6th International Electric Vehicle Technology Conference, 2023.
[23]M. Marinelli, L. Calearo, J. Engelhardt, and G. Rohde, "Electrical Thermal and Degradation Measurements of the LEAF e-plus 62-kWh Battery Pack," in Proceedings of 2022 International Conference on Renewable Energies and Smart Technologies IEEE, 2022.